Superconducting instability in the infinite-U Anderson lattice in the presence of crystal electric fields

B. R. Trees*
Department of Physics, The Ohio State University, 174 W. 18th Ave., Columbus, Ohio 43210
(Received 23 May 1994; revised manuscript received 12 July 1994)

We have studied the mean-field quasiparticle states and quasiparticle interactions in the infinite-U Anderson lattice in the presence of crystal electric fields of cubic symmetry. We assume a lattice of $4f$ sites, each with a total angular momentum of $J = 5/2$ that is split into a low-lying doublet of Γ_7 symmetry and an excited quartet of Γ_8 symmetry. Slave bosons on the $4f$ sites create and destroy $4f^0$ configurations and Lagrange multipliers at each $4f$ site enforce the occupancy constraint due to the infinite Coulomb repulsion. The quasiparticle states are strongly peaked at the points where the Fermi surface intersects the axes of the cubic Brillouin zone, leading to what we call "hot spots." We have calculated the effective magnetic moment and the Wilson ratio for these anisotropic quasiparticle states. Quasiparticle interactions are due to exchange of $4f$ density fluctuations. We use the analytic tetrahedron method to calculate the dressed (to order 1/N) boson Green functions. In weak coupling, the exchange of the dressed bosons gives rise to a superconducting instability of T_{1g}, $xy(x^2 - y^2)$, symmetry. The A_{1g}, "s-wave," channel has strongly repulsive interactions and hence no pairing instability. The T_{2g} channel exhibits weakly repulsive interactions. Average quasiparticle interactions in the E_g, $x^2 - y^2$, $3z^2 - r^2$, channel fluctuate strongly as a function of the number of tetrahedra used to calculate the bosonic Green functions, lending only weak evidence for an instability of E_g symmetry.

I. INTRODUCTION

This paper is concerned with the effects of crystal electric fields on quasiparticle interactions in the Ce-based heavy fermion superconductor $CeCu_2Si_2$ [$T_c \approx 0.6$ K (Ref. 1)]. In general, the heavy fermion materials are examples of systems exhibiting strong correlations among the constituent particles.[2–7] The compounds are comprised of intermetallics and rare-earth or actinide atoms (such as uranium or cerium) with a strong on-site Coulomb repulsion. This large electrostatic energy arises from the localized nature of the $4f$ or $5f$ wave functions in the solid and markedly influences the electron occupation at these "rare-earth" sites. When hybridization between a rare-earth electron and a conduction electron is allowed, the physics of this strong interaction is communicated to the solid at large, giving rise to a metal of strongly correlated, interacting electrons. In such a system one might expect to find a ground state manifesting collective properties of the coupled rare-earth and conduction electrons, e.g., superconductivity or magnetism. Indeed such ground states are seen. There are also heavy fermion systems that apparently retain a metallic state down to zero temperature. To date there are six known heavy fermion superconductors, all containing either cerium or uranium.

Our work is based on the infinite-U Anderson lattice, the details of which we shall discuss later. For the experts, we mention here that we use slave boson operators to create or destroy $4f^0$ configurations on the Ce sites, thereby avoiding the cumbersome Hubbard operators in the hybridization piece of the Hamiltonian.[8–10] There is also a Lagrange multiplier to enforce unit occupancy of the $4f$ multiplets at each Ce site. In our work we also include, at the Ce sites, crystal electric fields of cubic symmetry, which has the effect of splitting the spin-orbit-coupled ($J = 5/2$) multiplet into a doublet (of Γ_7 symmetry) and a quartet (of Γ_8 symmetry). We take the Γ_7 doublet to be the ground multiplet, with a crystal field splitting Δ_{CEF} to the Γ_8 quartet that is much larger than the Kondo temperature of the low-lying doublet, T_{07} ($\Delta_{CEF} \gg T_{07}$).

Previous theoretical work has focused on understanding the heavy fermion compounds mainly through the SU(N) version of the periodic Anderson model,[11–15] in which each $4f$ multiplet is N-fold degenerate, and the (plane-wave) conduction bands are assumed to be N-fold degenerate as well. The matrix element $V(\mathbf{k})$, for hybridization between a conduction electron and a $4f$ electron, is taken to be isotropic in momentum space.

Within the SU(N) model, Lavagna, Millis, and Lee[15] and Auerbach and Levin[12] have studied quasiparticle interactions due to the exchange of $4f$ density fluctuations. The lowest-order diagrams contributing to the interactions are of order $1/N$, where N is the $4f$ multiplet degeneracy. In Ce, in the absence of crystal field splitting, the low-lying $J = 5/2$ multiplet is sixfold degenerate ($N = 6$). So it seems reasonable to truncate the diagrams at order $1/N$. Lavagna, Millis, and Lee found that such a spinless density exchange yielded a d-wave superconducting instability in the spin-singlet pairing channel. Houghton, Read, and Won[16] extended these results by calculating $1/N^2$ contributions to the scattering amplitude, thus including quasiparticle interactions due to the exchange of spin as well as charge fluctua-

tions. They discovered that attractive interactions, even at order $1/N^2$, could be strong enough to yield pairing instabilities in either the p- or d-wave channels. In fact, when they compared the strengths of the pairing interactions due to charge and spin fluctuations separately, they concluded that for typical values of N and m^*/m (m^* is the quasiparticle effective mass and m is the mass of a free electron) spin-fluctuation-mediated pairing should dominate. It is clear that a $1/N^2$ calculation, including spin fluctuations, should be performed in the case of crystal-field-split multiplets. Such a calculation would allow us to compare the relative strengths of charge versus spin-fluctuation-mediated interactions. The numerics required, however, are formidable at present, and so we have limited ourselves to order $1/N$.

Zhang and Lee[17] have performed a more realistic calculation at the $1/N$ level (as far as heavy fermion compounds are concerned) by including spin-orbit coupling at the Ce sites and by returning to twofold degenerate conduction states. They included an anisotropic hybridization matrix element, of the Coqblin-Schrieffer form,[18] between conduction and $4f$ electrons. These spin-orbit coupled ions are assumed to sit in an overall spherically symmetric "host" (as in a jellium model). Unlike in the SU(N) model, in the even-parity pairing channel, Zhang and Lee found *no* superconducting instabilities of s-wave, d-wave, or g-wave symmetry. It is worth noting here that the mean-field quasiparticle energy bands Zhang and Lee found are the same as those calculated by Zou and Anderson,[19] who used the Korringa-Kohn-Rostoker (KKR) scheme and included spin-orbit coupling on the $4f$ sites.

We have calculated both the mean-field quasiparticle states and density-fluctuation-induced quasiparticle interactions in the presence of crystal electric field splitting of the Ce $J = 5/2$ multiplets. At the intersection of the Fermi surface with the axes of the cubic Brillouin zone, the quasiparticle states are strongly peaked. This is due to the vanishing of the hybridization between the plane-wave conduction and the crystal field states of Γ_7 symmetry. We call these points "hot spots" and have calculated the effective magnetic moment and Wilson ratio in their presence. Density-fluctuation-induced quasiparticle interactions are calculated from the particle-particle scattering amplitude. We find that the anisotropy due to cubic symmetry qualitatively and quantitatively alters the interactions in comparison to the jellium model results of Zhang and Lee. In fact, we find evidence (at order $1/N$) for a superconducting instability of T_{1g} [$xy(x^2-y^2)$] symmetry in the even-parity pairing channel. We also find weaker evidence for an E_g ($x^2 - y^2$) pairing instability. We find *no* instability in the A_{1g} (the "s wave" of cubic symmetry) channel, which is not surprising, given the strong on-site Coulomb repulsion built into the Anderson model. The results of Houghton, Read, and Won strongly suggest that spin fluctuation exchange (order $1/N^2$) should be included as well. We wish to emphasize that, as we shall discuss, difficulties already at order $1/N$ precluded us from evaluating $1/N^2$ diagrams in the presence of crystal-field-split multiplets.

We also wish to note that the application of a $1/N$ expansion in the presence of a low-lying doublet (N=2) has been discussed by several authors.[20,21] (See also the discussion in Ref. 22.) It has been shown that ground state properties of the Anderson impurity model as calculated from Bethe ansatz techniques show excellent agreement with $1/N$ results even for N=2. Furthermore, the $1/N$ expansion is easily generalized to the case of a lattice of rare-earth ions, as applies here, and gives a controlled procedure for evaluating diagrams.

The details of our calculation are presented here as follows. In Sec. II, we introduce the Hamiltonian for the infinite-U Anderson lattice in the presence of crystal fields. The Hamiltonian formalism shall be retained throughout this paper, as opposed to functional integral techniques.[9,12,14,15,23] In Sec. III, we discuss the mean-field properties of our Hamiltonian, including the quasiparticle energies and states, and in Sec. IV we discuss our calculation of the Wilson ratio. In Sec. V, we discuss our calculation of the dressed slave boson Green functions, which includes the effects of particle-hole excitations in the hybridization coupled conduction and $4f$ electron system. We also briefly explain our use of the analytic tetrahedron method for performing the complicated three-dimensional Brillouin zone integrals that arise in the evaluation of the particle-hole diagrams. Finally, in Secs. VI and VII, we present our results for the superconducting instabilities in the presence of cubic symmetry, which are based on the Fermi surface average of the quasiparticle-quasiparticle scattering amplitude.

II. HAMILTONIAN

We assume a crystal electric field splitting of the $4f^1$ states consistent with an effective cubic symmetry at the Ce sites. Such a choice is based on the specific heat data of Bredl *et al.*[24] for $CeCu_2Si_2$ and is consistent with bulk susceptibility measurements[25] and the isotropy of the slope of the upper critical field at T_c, $H'_{c2}(T_c)$.[26] Initial evidence of crystal electric field splitting in $CeCu_2Si_2$ by inelastic neutron scattering was found by Horn *et al.*[27]

In the presence of cubic symmetry, the J=5/2 multiplet is split into a doublet of Γ_7 symmetry and a Γ_8 quartet.[28] The crystal-field-split states $|\Gamma\alpha\rangle$, where α labels the degenerate states for a given multiplet, are a linear combination of the eigenstates of the z component of the total angular momentum $|m\rangle$, where $-5/2 \leq m \leq 5/2$,

$$|\Gamma\alpha\rangle = \sum_m c_{\Gamma\alpha m}|m\rangle. \quad (1)$$

The coefficients $c_{\Gamma\alpha m}$ are given in Table I. Based on the experimental data mentioned in the previous paragraph, we assume a Γ_7 doublet ground state, with a crystal field splitting to a Γ_8 quartet of Δ_{CEF}=31.5 meV.

The matrix element $V_{\Gamma\alpha\sigma}(\mathbf{k})$ represents hybridization between a crystal field state with quantum numbers Γ, α and a plane-wave conduction state with crystal momentum $\mathbf{k}$ and spin σ. In the case of a single ion in the full J=5/2 manifold, one may use the Coqblin-Schrieffer[18] matrix element

TABLE I. Crystal-field-split states as a linear combination of the eigenstates of the z component of the total angular momentum $|m\rangle$, where $-5/2 \leq m \leq 5/2$.

$$|\Gamma_7,+1\rangle = -\sqrt{\tfrac{1}{6}}|-\tfrac{5}{2}\rangle + \sqrt{\tfrac{5}{6}}|\tfrac{3}{2}\rangle$$
$$|\Gamma_7,-1\rangle = -\sqrt{\tfrac{1}{6}}|\tfrac{5}{2}\rangle + \sqrt{\tfrac{5}{6}}|-\tfrac{3}{2}\rangle$$
$$|\Gamma_8,+2\rangle = \sqrt{\tfrac{5}{6}}|\tfrac{5}{2}\rangle + \sqrt{\tfrac{1}{6}}|-\tfrac{3}{2}\rangle$$
$$|\Gamma_8,+1\rangle = |\tfrac{1}{2}\rangle$$
$$|\Gamma_8,-1\rangle = |-\tfrac{1}{2}\rangle$$
$$|\Gamma_8,-2\rangle = \sqrt{\tfrac{5}{6}}|-\tfrac{5}{2}\rangle + \sqrt{\tfrac{1}{6}}|\tfrac{3}{2}\rangle$$

$$V_{m\sigma}(\mathbf{k}) = -\sqrt{\frac{4\pi}{3}}(-i)^3\sigma V_{0k}\sqrt{\frac{7-2m\sigma}{14}}Y^*_{3,m-\frac{\sigma}{2}}(\hat{k}), \tag{2}$$

where $\sigma=\pm1$ is the (pseudo)spin index. V_{0k} denotes the dependence of the hybridization strength on the *magnitude* of the momentum, which will be important only near the zone center. In fact, we can write $V_{0k}=V_0 g(k)$, where $g(k)$ is a function of $|\mathbf{k}|$ that goes to zero on approaching the zone center like k^3. V_0 is the bare hybridization strength. Because the crystal-field-split $4f$ states are just linear combinations of the $J=5/2$ states, the hybridization matrix elements in cubic symmetry are

$$V_{\Gamma\alpha\sigma}(\mathbf{k}) = \sum_{m=-5/2}^{m=5/2} c_{\Gamma\alpha m} V_{m\sigma}(\mathbf{k}). \tag{3}$$

Next, we say a few words on the important energy scales of $CeCu_2Si_2$, based on the discussion of Kang *et al.*[29] on the electron spectroscopic data available as of 1990. They analyzed their own data of the Ce $3d$ x-ray photoelectron spectrum (XPS) and $4f$ bremsstrahlung isochromat spectrum (BIS); they also analyzed the Ce $4f$ resonant photoelectron data (RESPES) of Parks *et al.*[30] Kang and co-workers calculated the appropriate one-electron spectra from the impurity Anderson model, which showed reasonably good agreement with the data. On the basis of such a calculation, the authors claim that Coulomb energy for double occupation of a Ce $4f$ site is $U \approx 7$ eV.

The large Coulomb energy for $CeCu_2Si_2$ prompts us to take the limit in which U goes to infinity, thereby forbidding hybridization processes that give rise to $4f^1 \rightarrow 4f^2$ valence fluctuations. This is a technical simplification for us, but even though U is indeed very large by solid-state physics standards, it may be that the physics of finite U is crucial to the understanding of heavy fermions. Recently Cox[31] has proposed the quadrupolar Kondo model (or two-channel Kondo model) as an explanation of the superconductivity and of the possible non-Fermi liquid behavior in uranium-based heavy fermions. Nevertheless, the infinite-U limit is a reasonable simplification (at least for $CeCu_2Si_2$) of an already difficult problem and warrants study in its own right.

Our Hamiltonian can be written as a combination of terms: $H = H_c + H_f + H_{\rm mix} + H_{\rm constraint}$. The kinetic energy of the conduction electrons is given by

$$H_c = \sum_{\mathbf{k}\sigma} \xi_{\mathbf{k}} c^\dagger_{\mathbf{k}\sigma} c_{\mathbf{k}\sigma}, \tag{4}$$

where

$$\xi_{\mathbf{k}} = \frac{\hbar^2 k^2}{2m} - \mu_0, \tag{5}$$

is the plane-wave dispersion. The zero of energy for this calculation will be taken with respect to μ_0, the chemical potential of the conduction electrons in the absence of hybridization.

The $4f$ electron site energy is

$$H_f = \sum_{\mathbf{R}\Gamma\alpha} E_\Gamma f^\dagger_{\mathbf{R}\Gamma\alpha} f_{\mathbf{R}\Gamma\alpha}, \tag{6}$$

where $\mathbf{R}$ is the site index in real space, and $\Gamma\alpha$ are the crystal field quantum numbers. The operator $f_{\mathbf{R}\Gamma\alpha}$ destroys a $4f^1$ configuration at lattice site $\mathbf{R}$, in which the crystal field state $\Gamma\alpha$ is initially occupied. From the photoemission data,[29] we take the energy of the Γ_7 doublet to be -2.0 eV, i.e., $E_7 = -2.0$ eV. From the inelastic neutron scattering data[27] and the high-temperature specific heat,[24] we take the Γ_8 level to lie 31.5 meV (≈ 360 K) above the Γ_7 level,

$$E_8 = E_7 + \Delta_{\rm CEF} = -1.964 \text{ eV}. \tag{7}$$

The hybridization, or mixing, term is

$$H_{\rm mix} = \frac{1}{\sqrt{N_s}} \sum_{\mathbf{k}\sigma\mathbf{R}\Gamma\alpha} \left[V_{\Gamma\alpha\sigma}(\mathbf{k}) c^\dagger_{\mathbf{k}\sigma} f_{\mathbf{R}\Gamma\alpha} b^\dagger_{\mathbf{R}} e^{i\mathbf{k}\cdot\mathbf{R}} + \text{H.c.} \right]. \tag{8}$$

The operator $b^\dagger_{\mathbf{R}}$ is a slave boson creation operator, which creates a $4f^0$ configuration, or hole, at lattice site $\mathbf{R}$. N_s is the number of lattice sites. This combination of conduction, $4f$, and slave boson operators was first applied to the Anderson model by Barnes,[8] and was later reintroduced by Coleman.[10] $H_{\rm mix}$ contains only bosonic or fermionic operators, and so Wick's theorem is applicable. Use of the more cumbersome Hubbard projection operators,

$$X_{0\Gamma\alpha} = |0\rangle\langle\Gamma\alpha| \tag{9}$$

would make Feynman diagrammatic procedures invalid, since the Hubbard operators do not obey standard commutation relations. The cubic symmetry is reflected in the structure of the anisotropic function $V_{\Gamma\alpha\sigma}(\mathbf{k})$, which has a significantly different $\mathbf{k}$ dependence than the Coqblin-Schrieffer form $V_{m\sigma}(\mathbf{k})$. This new anisotropy will affect quasiparticle interactions differently than in the case of spherical symmetry.

Finally, there is the constraint term, which is introduced with a Lagrange multiplier $i\lambda_{\mathbf{R}}$, ensuring that the *total* occupancy (fermions plus bosons) at the Ce sites is unity,

$$H_{\rm constraint} = \sum_{\mathbf{R}} i\lambda_{\mathbf{R}} \left(f^\dagger_{\mathbf{R}\Gamma\alpha} f_{\mathbf{R}\Gamma\alpha} + b^\dagger_{\mathbf{R}} b_{\mathbf{R}} - Q \right). \tag{10}$$

Note that Q=1 is the physically meaningful value in this case.

As discussed in Refs. 9 and 11, the slave boson operator can be written in terms of an amplitude and a phase. We let $s_{\mathbf{R}}$ be the amplitude of the boson at site $\mathbf{R}$. The Bose propagator is then a 2×2 matrix, which in the static limit will have elements composed of averages over the Bose amplitude and the Lagrange multiplier: ss, $s\lambda$, and $\lambda\lambda$.

In the SU(N) case, in order to have a well-defined Kondo temperature in the limit of large N, it was necessary to assume the bare hybridization strength V_0 scaled like $1/\sqrt{N}$.[11] We do the same here by defining a rescaled hybridization matrix element,

$$\tilde{V}_{\Gamma\alpha\sigma}(\mathbf{k}) \equiv \sqrt{N_\Gamma} V_{\Gamma\alpha\sigma}(\mathbf{k}), \tag{11}$$

where we assume that $\tilde{V}_{\Gamma\alpha\sigma}(\mathbf{k})$ is of order 1. Note that N_Γ is the degeneracy of the Γ crystal field multiplet. Also, because the hybridization matrix element and the boson operator $s_{\mathbf{R}}$ appear together in $H_{\rm mix}$, we define a scaled boson operator

$$\tilde{s}_{\mathbf{R}\Gamma} \equiv \frac{s_{\mathbf{R}}}{\sqrt{N_\Gamma}}, \tag{12}$$

where we assume that $\tilde{s}_{\mathbf{R}\Gamma}$ is also of order 1.

III. MEAN-FIELD APPROXIMATION

In this section, we discuss the properties of our Hamiltonian at the mean-field level, where we assume that both the Bose operator and the Lagrange multiplier are uniform in space. In this limit, the Hamiltonian in k space takes the following form:

$$\begin{aligned} H_{\rm MF} = &\sum_{\mathbf{k}\sigma} \xi_{\mathbf{k}} c^\dagger_{\mathbf{k}\sigma} c_{\mathbf{k}\sigma} + \sum_{\mathbf{k}\Gamma\alpha} \epsilon_\Gamma f^\dagger_{\mathbf{k}\Gamma\alpha} f_{\mathbf{k}\Gamma\alpha} \\ &+ \sum_{\mathbf{k}\sigma\Gamma\alpha} \left[\tilde{s}_{0\Gamma} \tilde{V}_{\Gamma\alpha\sigma}(\mathbf{k}) c^\dagger_{\mathbf{k}\sigma} f_{\mathbf{k}\Gamma\alpha} + \text{H.c.} \right] \\ &+ \frac{N_s}{2} \sum_\Gamma N_\Gamma i\lambda_0 \left(\tilde{s}^2_{0\Gamma} - q_{0\Gamma} \right) \end{aligned} \tag{13}$$

where $\epsilon_\Gamma \equiv E_\Gamma + i\lambda_0$ is the shifted energy of the Γ multiplet. We assume that $q_{0\Gamma}$ is of order 1, but technically, when it comes down to getting numerical results, we know that $q_{0\Gamma} = 1/N_\Gamma$. Note that $\tilde{s}_{0\Gamma}$ and λ_0 are the mean-field values of the Bose operator and Lagrange multiplier, respectively ($\tilde{s}_{0\Gamma} = s_0/\sqrt{N_\Gamma}$).

It is straightforward to diagonalize $H_{\rm MF}$ and obtain the quasiparticle states and energies. Because the Γ_8 states are fourfold degenerate, there is one nonhybridizing quasiparticle band of Γ_8 symmetry. The secular equation which gives the quasiparticle energies $E_{n\mathbf{k}}$ (n=1,2,3 is the band index) is

$$\begin{aligned} (\epsilon_8 - E_{n\mathbf{k}}) \Bigg[(\xi_{\mathbf{k}} - E_{n\mathbf{k}}) &- \sum_{\alpha_7} \frac{\tilde{s}^2_{07} |\tilde{V}_{7\alpha\sigma}|^2}{(\epsilon_7 - E_{n\mathbf{k}})} \\ &- \sum_{\alpha_8} \frac{\tilde{s}^2_{08} |\tilde{V}_{8\alpha\sigma}|^2}{(\epsilon_8 - E_{n\mathbf{k}})} \Bigg] = 0, \end{aligned} \tag{14}$$

where the sum $\sum_{\alpha_{7(8)}}$ means only the states in the $\Gamma_{7(8)}$ multiplet are summed. Although technically it is possible to find analytic solutions of Eq. (14), the analytic expressions are too cumbersome to be useful; thus we calculated the roots numerically. The three quasiparticles bands are plotted in Fig. 1 along two different directions in the cubic Brillouin zone. Figure 1 shows that along the axes of the zone, for example along the ΓX direction, the states of Γ_7 symmetry cannot hybridize with the conduction states. This means that the matrix elements $V_{7\alpha\sigma}(\mathbf{k})$ vanish along these special directions and that there is no gap between the first and second quasiparticle bands [see Fig. 1(b)]. Such behavior has been discussed by Martin.[32]

The quasiparticle states can, quite generally, be written as a combination of plane-wave and crystal field states,

$$|Q_{n\mathbf{k}\sigma}\rangle = A_n(\mathbf{k}) \left[|\mathbf{k}\sigma\rangle - \sum_{\Gamma\alpha} \frac{\tilde{s}_{0\Gamma} \tilde{V}^*_{\Gamma\alpha\sigma}(\mathbf{k})}{\epsilon_\Gamma - E_{n\mathbf{k}}} |\Gamma\alpha\rangle \right], \tag{15}$$

where $|\mathbf{k}\sigma\rangle$ is a plane-wave state. The *anisotropic* normalization function is

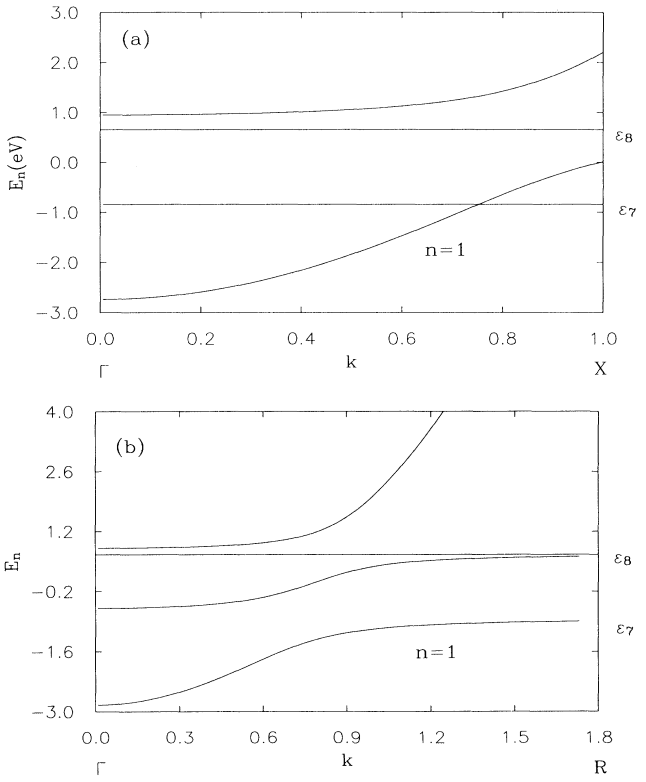

FIG. 1. Schematic of the quasiparticle band structure, showing the shifted crystal field multiplet energies (ϵ_7 and ϵ_8), the chemical potential (μ), and the lower band edge ($-D$). (a) The k values range from the zone center (the Γ point) to the intersection of the k_x axis with the cubic Brillouin zone boundary. (b) From the zone center to the intersection of a cube diagonal with the Brillouin zone boundary.

$$A_n^2(\mathbf{k}) = \left[1 + \frac{1}{2}\sum_{\Gamma\alpha\sigma} \frac{\tilde{s}_{0\Gamma}^2 |\tilde{V}_{\Gamma\alpha\sigma}(\mathbf{k})|^2}{(\epsilon_\Gamma - E_{n\mathbf{k}})^2}\right]^{-1}. \quad (16)$$

For given crystal field quantum numbers $\Gamma\alpha$, it is possible to sum over the pseudo-spin variable σ in Eq. (16). For convenience, we define a function

$$\mu_{\Gamma\alpha\Gamma'\alpha'}(\mathbf{k}) \equiv \sum_\sigma \tilde{V}^*_{\Gamma\alpha\sigma}(\mathbf{k})\tilde{V}_{\sigma\Gamma'\alpha'}(\mathbf{k}). \quad (17)$$

Then the sum over the pseudospin variable in the expression for $A_n^2(\mathbf{k})$ is just the diagonal element $\mu_{\Gamma\alpha\Gamma\alpha}(\mathbf{k})$. All possible (nonzero) forms for the function $\mu_{\Gamma\alpha\Gamma'\alpha'}(\mathbf{k})$ are shown in Table II, where the dependence on the *magnitude* of $\mathbf{k}$ has been divided out. Using the results of this table, it is possible to arrive at the following expression for the normalization function, which is valid at any point in the Brillouin zone:

$$A_1^2 = \frac{\left(\frac{T_{07}}{s_0 V_0}\right)^2}{\frac{1}{3} + \frac{2}{3}\left(\frac{T_{07}}{T_{08}}\right)^2 - \frac{2\sqrt{\pi}}{9}\left[1 - \left(\frac{T_{07}}{T_{08}}\right)^2\right]\left[Y_{40}(\hat{k}) + \sqrt{\frac{5}{14}}\left(Y_{44}(\hat{k}) + Y_{4-4}(\hat{k})\right)\right]}. \quad (18)$$

Figure 2 shows a plot of Eq. (18) along the equator of a spherical Fermi surface, with ϕ denoting the azimuthal angle measured with respect to a coordinate axis. The extremely sharp variations near the axes represent the vanishing of the Γ_7 hybridization matrix elements. The six points where the Brillouin zone axes intersect the Fermi surface we call "hot spots;" they must be handled with care when averaging the quasiparticle scattering amplitude over the Fermi surface.

We would like to remark that, in this model, the existence of hot spots is a manifestation of the lowering of the symmetry below spherical. In spherical symmetry, there is a sum rule for the matrix elements that renders the normalization function A^2 isotropic in k space.[15,17] In our case, the matrix elements cannot be simplified to an isotropic function. This means that hot spots can occur anywhere in the Brillouin zone where some subset of the hybridization matrix elements $\tilde{V}_{\Gamma\alpha\sigma}(\mathbf{k})$ vanishes.

TABLE II. Functional forms for the angular dependence of $\mu_{\Gamma\alpha\Gamma'\alpha'}$ for all possible combinations of the crystal field quantum numbers $\Gamma, \alpha, \Gamma', \alpha'$. Note that by time-reversal symmetry, $\mu_{\Gamma\alpha\Gamma'\alpha'} = \mu_{\Gamma^*\alpha^*\Gamma'^*\alpha'^*}$, where the asterisk denotes the time-reversed pair. For example, $\mu_{71,71} = \mu_{7,-1,7,-1}$. Note, also, that $V_{0\Gamma}(|\mathbf{k}|)$ represents the dependence of the hybridization strength on the radial component of $\mathbf{k}$. Any combination of quantum numbers not present in the table or not the time-reversed pair of quantum numbers in the table will vanish upon summing over the pseudospin indices.

Γ, α	Γ', α'	$\mu_{\Gamma\alpha\Gamma'\alpha'}(\mathbf{k})/\tilde{V}_{0\Gamma}(\lvert\mathbf{k}\rvert)\tilde{V}_{0\Gamma'}(\lvert\mathbf{k}\rvert)$
7,1	7,1	$-\frac{2\sqrt{\pi}}{3}\left[Y_{00} - \frac{1}{3}Y_{40} - \frac{1}{3}\sqrt{\frac{5}{14}}(Y_{44} + Y_{4-4})\right]$
8,2	8,2	$-\frac{2\sqrt{\pi}}{3}\left[Y_{00} - \frac{8}{7}\sqrt{\frac{1}{5}}Y_{20} + \frac{1}{21}Y_{40} + \frac{1}{3}\sqrt{\frac{5}{14}}(Y_{44} + Y_{4-4})\right]$
8,1	8,1	$-\frac{2\sqrt{\pi}}{3}\left[Y_{00} + \frac{8}{7}\sqrt{\frac{1}{5}}Y_{20} + \frac{2}{7}Y_{40}\right]$
8,2	8,1	$\frac{10}{21}\sqrt{\frac{2\pi}{5}}\left[Y_{22} + \frac{3}{5}Y_{2-2} - \frac{\sqrt{3}}{2}Y_{42} + \frac{\sqrt{3}}{6}Y_{4-2}\right]$
8,1	8,2	$\frac{10}{21}\sqrt{\frac{2\pi}{5}}\left[Y_{2-2} + \frac{3}{5}Y_{22} - \frac{\sqrt{3}}{2}Y_{4-2} + \frac{\sqrt{3}}{6}Y_{42}\right]$
8,2	8,-1	$-\frac{4}{21}\sqrt{\frac{2\pi}{5}}\left[Y_{2-1} + \frac{5}{6}\sqrt{\frac{3}{2}}Y_{4-1} - \frac{5}{6}\sqrt{\frac{21}{2}}Y_{43}\right]$
8,-1	8,2	$\frac{4}{21}\sqrt{\frac{2\pi}{5}}\left[Y_{21} + \frac{5}{6}\sqrt{\frac{3}{2}}Y_{4-1} - \frac{5}{6}\sqrt{\frac{21}{2}}Y_{4-3}\right]$
7,1	8,2	$\frac{4}{21}\sqrt{6\pi}\left[Y_{2-1} - \sqrt{\frac{1}{6}}Y_{4-1}\right]$
8,2	7,1	$-\frac{4}{21}\sqrt{6\pi}\left[Y_{21} - \sqrt{\frac{1}{6}}Y_{41}\right]$
7,1	8,1	$-\frac{4}{21}\sqrt{2\pi}\left[Y_{21} + \frac{1}{6}\sqrt{\frac{21}{2}}Y_{4-3} + \frac{5}{6}\sqrt{\frac{3}{2}}Y_{41}\right]$
8,1	7,1	$-\frac{4}{21}\sqrt{2\pi}\left[Y_{2-1} + \frac{1}{6}\sqrt{21}2Y_{43} + \frac{5}{6}\sqrt{\frac{3}{2}}Y_{4-1}\right]$
7,1	8,-1	$\frac{2}{21}\sqrt{18\pi}\left[Y_{22} - \frac{1}{3}Y_{2-2} + \frac{1}{2\sqrt{3}}Y_{4-2} + \frac{5}{6\sqrt{3}}Y_{42}\right]$
8,-1	7,1	$\frac{2}{21}\sqrt{18\pi}\left[Y_{2-2} - \frac{1}{3}Y_{22} + \frac{1}{2\sqrt{3}}Y_{42} + \frac{5}{6\sqrt{3}}Y_{4-2}\right]$
7,1	8,-2	$-\frac{4}{21}\sqrt{\pi}\left[Y_{20} - \frac{\sqrt{5}}{3}Y_{40} + \frac{5}{6}\sqrt{\frac{7}{2}}Y_{4-4} - \frac{1}{6}\sqrt{\frac{7}{2}}Y_{44}\right]$
8,-2	7,1	$-\frac{4}{21}\sqrt{\pi}\left[Y_{20} - \frac{\sqrt{5}}{3}Y_{40} + \frac{5}{6}\sqrt{\frac{7}{2}}Y_{44} - \frac{1}{6}\sqrt{\frac{7}{2}}Y_{4-4}\right]$

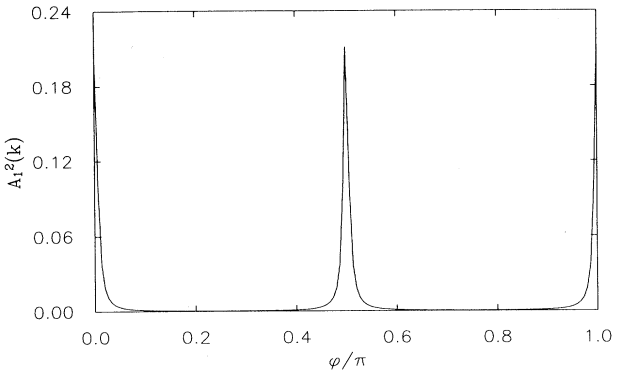

FIG. 2. A plot of the normalization function $A_1^2(\mathbf{k})$ along the equator of a sphere in k space as a function of azimuthal angle ϕ. The sharp spikes occur at the intersections of the equator with the coordinate axes. At these points the Γ_7 hybridization matrix elements vanish exactly, and the width of these peaks is set by the ratio of the two Kondo temperatures $T_{07}/T_{08} \approx T_{07}/\Delta_{\mathrm{CEF}}$. The behavior for a fixed azimuthal angle (ϕ=0) as a function of the polar angle θ is the same.

This is a rather general statement that relies only on the symmetry being lower than spherical and should not be unique to cubic lattices.

We can relate the fermionic creation and destruction operators in the original basis (the c and f operators) to creation and destruction operators in the quasiparticle basis, $Q^\dagger_{\mathbf{k}n\sigma}$, $Q_{\mathbf{k}n\sigma}$. We find that

$$c_{\mathbf{k}\sigma} = \sum_n A_n(\mathbf{k}) Q_{\mathbf{k}n\sigma}, \tag{19}$$

$$f_{\mathbf{k}\Gamma\alpha} = -\sum_{n\sigma} \frac{A_n(\mathbf{k})\tilde{s}_{0\Gamma}\tilde{V}^*_{\Gamma\alpha\sigma}(\mathbf{k})}{\epsilon_\Gamma - E_{n\mathbf{k}}} Q_{\mathbf{k}n\sigma}. \tag{20}$$

These expressions are useful in constructing the two-quasiparticle scattering amplitude.

In the last part of this section, we discuss the self-consistency equations that arise when one demands that the free energy in the mean-field approximation be an extremum with respect to the Bose fields s_0 and $i\lambda_0$. Since we have diagonalized the mean-field Hamiltonian, Eq. (13), we can write it in terms of the quasiparticle energies and operators:

$$H_{\mathrm{MF}} = \sum_{\mathbf{k}n\sigma} E_{n\mathbf{k}} Q^\dagger_{\mathbf{k}n\sigma} Q_{\mathbf{k}n\sigma} + \frac{N_s}{2}\sum_\Gamma N_\Gamma i\lambda_0\left(\tilde{s}^2_{0\Gamma} - q_{0\Gamma}\right). \tag{21}$$

The corresponding mean-field free energy has the form

$$F_{\mathrm{MF}} = \frac{N_s}{2}\sum_\Gamma N_\Gamma i\lambda_0\left(\tilde{s}^2_{0\Gamma} - q_{0\Gamma}\right) - \frac{1}{\beta}\sum_{\mathbf{k}n\sigma}\ln\left(1 + e^{-\beta E_{n\mathbf{k}}}\right), \tag{22}$$

where β is the inverse temperature. Requiring that $\partial F_{\mathrm{MF}}/\partial i\lambda_0 = 0$ and $\partial F_{\mathrm{MF}}/\partial s_0 = 0$ yields the equations

$$\frac{1}{2}\sum_\Gamma N_\Gamma\left(\tilde{s}^2_{0\Gamma} - q_{0\Gamma}\right) + \frac{1}{N_s}\sum_{\mathbf{k}\sigma n} f(E_{n\mathbf{k}})\frac{\partial E_{n\mathbf{k}}}{\partial i\lambda_0} = 0 \tag{23}$$

and

$$2i\lambda_0 s_0 + \frac{1}{N_s}\sum_{\mathbf{k}\sigma n} f(E_{n\mathbf{k}})\frac{\partial E_{n\mathbf{k}}}{\partial s_0} = 0. \tag{24}$$

In Eqs. (23) and (24), $f(E_{n\mathbf{k}})$ is the Fermi function evaluated at the quasiparticle energy $E_{n\mathbf{k}}$. We also need an equation to fix the chemical potential of the *quasiparticles* μ, which depends on the total number of electrons (conduction electrons, n_c, and f electrons, n_f) per unit cell,

$$n_{\mathrm{total}} = n_c + n_f = \frac{1}{N_s}\sum_{\mathbf{k}\sigma n} f(E_{n\mathbf{k}}). \tag{25}$$

These three coupled integral equations, when solved self-consistently, give the shifted $4f$ multiplet energies ϵ_Γ, the value of the Bose field s_0, and the quasiparticle chemical potential μ. The input parameters are n_{total}, the total filling factor, the bare hybridization strength V_0, and the conduction electron filling factor n_c. The zero of energy is always measured relative to the chemical potential of the *conduction* electrons, μ_0. For n_{total} =2, the lowest quasiparticle band is completely filled, and the system is a Kondo insulator. We have consistently used n_{total} =1.5, which ensures that we have a metal.

To get numerical self-consistent solutions, we found it necessary to write these equations in terms of energy integrals with the appropriate density of states,

$$\frac{1}{N_s}\sum_{\mathbf{k}\sigma} \to 2\int d\xi N(\xi)\int\frac{d\Omega}{4\pi}, \tag{26}$$

where $N(\xi)$ is the density of states per spin for the unhybridized conduction electrons and $d\Omega$ is an element of the solid angle. Note that in the SU(N) model described previously, the spin degeneracy would contribute a prefactor of N (instead of 2) in Eq. (26). For free electrons in three dimensions the density of states is proportional to the square root of ξ.

To proceed, we make one approximation. We assume that surfaces of constant energy for the quasiparticle states are spherically symmetric. Near the zone center, this is exactly correct, and there is no approximation at all. Near the zone boundary, the equal-energy surfaces become distorted from spheres due to the constraints of Γ_7 symmetry. It is important to note, however, that in Eqs. (23), (24), and (25), the *strongest* angular dependence comes from the anisotropic matrix elements, which we treat *exactly*. That is, we believe the angular dependence of the quasiparticle bands is not as important as that of the hybridization matrix elements. For example, near an axis of the Brillouin zone, the Γ_7 matrix elements are going to zero. So, even if the quasiparti-

cle energies surfaces are distorted from spheres near the axes, the sensitivity of the self-consistency equations to this distortion would be lessened by the presence of the small $V_{7\alpha\sigma}$ terms in the numerator. Thus, it should be a reasonable approximation to treat the mixing matrix elements as having all the angular dependence.

Using the secular equation for the quasiparticle band energies, Eq. (14), we can calculate all the necessary derivatives of the quasiparticle energies found in Eqs. (23) and (24). After averaging the anisotropic matrix elements over the Fermi surface, we are left with the following three equations to be solved self-consistently:

$$\frac{1}{2}\sum_{\Gamma} N_{\Gamma}\left(\tilde{s}_{0\Gamma}^2 - q_{0\Gamma}\right) + 2\frac{s_0^2 V_{k0}^2}{3}\int_{-D}^{\mu} dE N\big(\xi(E)\big)\left[\frac{1}{(\epsilon_7 - E)^2} + \frac{5}{(\epsilon_8 - E)^2}\right] = 0, \tag{27}$$

$$2i\lambda_0 - 2\frac{V_{k0}^2}{3}\int_{-D}^{\mu} dE N\big(\xi(E)\big)\left[\frac{1}{\epsilon_7 - E} + \frac{5}{\epsilon_8 - E}\right] = 0, \tag{28}$$

$$n_{\text{total}} - 2\int_{-D}^{\mu} dE N\big(\xi(E)\big)\left[1 + \frac{1}{3}\frac{s_0^2 V_{0k}^2}{(\epsilon_7 - E)^2} + \frac{5}{3}\frac{s_0^2 V_{0k}^2}{(\epsilon_8 - E)^2}\right], \tag{29}$$

where $-D$ is the energy at the bottom of the lowest quasiparticle band.

We have taken the limit of zero temperature to arrive at Eqs. (27)–(29). As a consequence, only the first quasiparticle band E_1 contributes at mean-field; for simplicity, we have dropped the band subscript 1. We consider two different sets of solutions, corresponding to the *conduction* electron filling factors of n_c =0.5 [which we call set (a)] and n_c =0.8 [which we call set (b)]. We define a Kondo temperature in the lattice for both Γ_7 and Γ_8 multiplets by

$$T_{0\Gamma} \equiv \epsilon_{\Gamma} - \mu. \tag{30}$$

The reader is reminded that μ is the *quasiparticle* chemical potential. The motivation for defining the Kondo temperature as the difference between the shifted multiplet energy (ϵ_Γ) and the quasiparticle chemical potential is that in the SU(N) model this difference has exactly the same structure as the Kondo temperature for the impurity problem. That is, in the SU(N) model, one finds that[33]

$$\epsilon - \mu = De^{-|E_f|/NN(0)V_0^2}, \tag{31}$$

where D is the half bandwidth, $N(0)$ is the (assumed flat) conduction electron density of states, E_f is the *unshifted* or bare $4f$ multiplet energy, and V_0 is the bare hybridization strength. All self-consistent mean-field parameters are presented in Table III. Note that both parameter sets (a) and (b) have approximate Kondo temperatures (for the Γ_7 doublet) of 10 K, which, based on the neutron scattering quasielastic linewidth,[27] is a reasonable estimate for $CeCu_2Si_2$. Note, also, that the Kondo temperature for the Γ_8 quartet is dominated by crystal field splitting,

$$T_{08} = T_{07} + \Delta_{\text{CEF}} \approx 370 \text{ K}, \tag{32}$$

where T_{07}/T_{08} ≈0.027. Figure 3 plots the lowest quasi-

TABLE III. Self-consistent mean-field parameter sets, labeled as (a) and (b). At mean field there are three coupled integral equations, which are solved self-consistently. The input parameters are the bare hybridization strength V_0; the lower edge of the conduction electron band in the absence of hybridization, $-D$; the total number of electrons, $n_{\text{total}} = n_{\text{cond}} + n_f$, per unit cell; the bare, or unshifted, energy of the Γ_7 (E_7) and the Γ_8 ($E_8 = E_7 + \Delta_{\text{CEF}}$) multiplets; and the fixed crystal field splitting Δ_{CEF} = 360 K. The self-consistent parameters which solve the equations are the hybridization renormalization coefficient s_0, where the mean-field-renormalized hybridization is s_0V_0; the shifted Γ_7 (ϵ_7) and Γ_8 ($\epsilon_8 = \epsilon_7 + \Delta_{\text{CEF}}$) multiplet energies; the *quasiparticle* chemical potential μ; and the Kondo temperature $T_{07} \equiv \epsilon_7 - \mu$ of the Γ_7 doublet. In both parameters sets (a) and (b), the total number of particles was fixed at n_{total}=1.5. And the input parameters were chosen to give approximate Kondo temperatures of 10 K, i.e., T_{07} ≈10 K. *All energies are measured relative the chemical potential in the absence of hybridization.* In both parameter sets, Δ_{CEF}=360 K, and the unshifted Γ_7 energy is $E_7 = -2.0$ eV.

Parameter set	V_0 (eV)	s_0	ϵ_7 (eV)	μ (eV)	T_{07} (K)	D (eV)
(a)	0.8595	0.093472	0.0217648	0.0208399	9.25	2.4405
(b)	0.650	0.142409	-0.8437021	-0.844999	13.0	3.33856

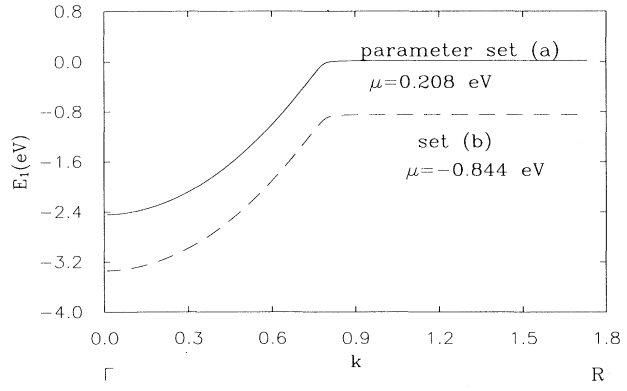

FIG. 3. Plot of the lowest energy band $E_{1\mathbf{k}}$ for the two mean-field parameter sets [labeled as (a) and (b)]. In set (a), the conduction electron chemical potential is 2.44 eV, and in set (b), it is 3.33 eV. Note that the bands are just shifted with respect to each other. For both parameter sets the unshifted Γ_7 multiplet energy sits at −2.0 eV.

particle bands for both mean-field parameter sets (a) and (b). The top of the first quasiparticle band is just below the shifted Γ_7 energy ϵ_7. The *quasiparticle* chemical potential cuts through the flat part of the first band in both cases, giving rise to a very large quasiparticle density of states at the Fermi surface.

IV. EFFECTIVE MAGNETIC MOMENT AND WILSON RATIO

In this section we discuss our results for the effective magnetic moment of the quasiparticle states when averaged over the Fermi surface. The quasiparticle states are given by Eq. (15), where the local crystal field states are orthonormal to each other. Note that in this case the dispersionless band lies at an energy $T_{07}+\Delta_{\mathrm{CEF}}$ above the Fermi energy, where the crystal field splitting is much larger than the Kondo temperature of the Γ_7 doublet, i.e., $T_{07} \ll \Delta_{\mathrm{CEF}}$. In order to calculate the effective magnetic moment, we need the following expectation value for the lowest quasiparticle band:

$$\langle Q_{\mathbf{k}1\sigma}|\hat{\mu}|Q_{\mathbf{k}1\sigma'}\rangle \equiv \mu_z^{\sigma\sigma'}(\mathbf{k}), \tag{33}$$

where the magnetic moment operator is

$$\hat{\mu}_z = \hat{l}_z + 2\hat{s}_z = g_J \hat{J}_z, \tag{34}$$

g_J being the g factor for total angular momentum J. We find that we can write Eq. (33) in the form

$$\mu_z^{\sigma\sigma'}(\mathbf{k}) = A_1^2(\mathbf{k})\left[\sigma\delta_{\sigma\sigma'} + \sum_{\Gamma'\alpha'\Gamma\alpha m} \frac{m g_J c_{\Gamma'\alpha' m} s_{0\Gamma'} V^*_{\Gamma'\alpha'\sigma}(\mathbf{k}) V_{\Gamma\alpha\sigma'}(\mathbf{k}) s_{0\Gamma} c_{\Gamma\alpha m}}{(\epsilon_{\Gamma'} - E_{1\mathbf{k}})(\epsilon_{\Gamma} - E_{1\mathbf{k}})}\right]. \tag{35}$$

As done by Zou and Anderson,[19] who calculated the effective moment in the absence of crystal field splitting, we average over the Fermi surface,

$$\mu^2_{\mathrm{cubic,eff}} = \int \frac{d\hat{k}}{4\pi}\left[\mu_z^{+1+1}(\mathbf{k})^2 + \mu_z^{+1-1}(\mathbf{k})^2\right]. \tag{36}$$

We find an average moment of

$$\mu^2_{\mathrm{cubic,eff}} = 0.583\mu_B^2, \tag{37}$$

for mean-field parameter set (a). For a free Γ_7 doublet the average moment is

$$\mu_7^2 = \frac{25}{49}\mu_B^2. \tag{38}$$

The effective magnetic moment in cubic symmetry is slightly larger than the value for a free Γ_7 moment. This was expected by Cox,[34] who predicted the effective moment would have the structure

$$\mu^2_{\mathrm{eff}} = \mu_7^2\left[1 + \alpha\sqrt{\frac{m}{m^*}}\right], \tag{39}$$

where α is a prefactor that could be as big as about 10. The contributions of order $\sqrt{m/m^*}$ come from the so-called hot spots. At these points on the Fermi surface, the plane-wave conduction states and the localized Γ_7 states cannot hybridize. Thus we expect the g factor at these spots to go back to the free electron value of 2, with the result that the contribution to μ_{eff} from the hot spots increases the effective moment above that of a free moment of Γ_7 symmetry. For parameter set (a), we have

$$\frac{m}{m^*} = \left(\frac{T_{07}}{s_0 V_0}\right)^2 = 1.33 \times 10^{-4}.$$

Equation (39) is applicable for the quoted values of μ^2_{eff} and μ_7^2 if α=9.23, which is a reasonable value.

Finally, we substitute μ^2_{eff} into the expression for the Wilson ratio,

$$R = \left(\frac{\pi k_B}{\mu_{\mathrm{eff}}}\right)^2 \frac{\chi(0)}{\gamma(0)}, \tag{40}$$

where $\chi(0)$ is the low-temperature susceptibility, $\gamma(0)$ is the linear coefficient of the specific heat, k_B is Boltzmann's constant, and μ_B is the Bohr magneton. Using $\chi(0)$=0.019 emu/mole (for a magnetic field along the c axis of the tetragonal unit cell),[35] and $\gamma(0)$=1000 mJ/(mole K^2) (Ref. 1) gives $R = 2.38$. We should note that reported results of approximately 0.5 for the Wilson ratio[3] are due to the use of the bare effective moment

$\mu_{\rm eff}=2.54\mu_B$ in Eq. (40). We also find it interesting to note that for the two-channel Kondo impurity, the Wilson ratio is approximately 2.6.

Zou and Anderson[19] calculated the effective quasiparticle magnetic moment in the absence of crystal field splitting, finding $\mu_{\rm eff}=1.08\mu_B$. Comparing this result with the value of the bare moment of an f^1 electron in a $J=5/2$ state, $\mu=2.54\mu_B$, they saw that hybridization had reduced the size of the moment. Thus the Pauli susceptibility

$$\chi_{\rm Pauli}=2\mu_{\rm eff}^2\tilde{N}(\mu), \tag{41}$$

where $\tilde{N}(\mu)=\frac{m^*}{m}N(\mu)$ is the enhanced density of states at the Fermi surface, was also affected. But Cox,[34] Zhang and Lee,[36] and Aeppli and Varma[37] pointed out that the presence of the dispersionless quasiparticle band lying at an energy equal to the Kondo energy above the Fermi surface meant that the corresponding Van Vleck (interband) term should be included in the susceptibility. This resulted in an effective magetic moment equal to that of a *bare* $J=5/2$ state. Crystal field splitting, in contrast, pushes this dispersionless quasiparticle band up to an energy of $\Delta_{\rm CEF}$ above the Fermi surface, where $\Delta_{\rm CEF}$ is more than an order of magnitude larger than the Kondo energy of the low-lying Γ_7 doublet. Thus ignoring the interband Van Vleck susceptibility is more justified in this case, and the Pauli susceptibility is dominated by the contribution from the Γ_7 states.

V. FLUCTUATIONS BEYOND MEAN FIELD

With the eigenstates of the mean-field Hamiltonian written in the undiagonalized basis, there are three fermionic Green functions: $G_{\Gamma\alpha\Gamma'\alpha'}$ (the f Green function), G_σ(the conduction Green function), and $G_{\Gamma\alpha\sigma}$(the off-diagonal, or mixing, Green function). All three are defined below in terms of Fock space operators:

$$G_{\Gamma\alpha\Gamma'\alpha'}(\mathbf{k},\tau)\equiv-\langle T_\tau f_{\mathbf{k}\Gamma\alpha}(\tau)f^\dagger_{\mathbf{k}\Gamma'\alpha'}(0)\rangle, \tag{42}$$

$$G_\sigma(\mathbf{k},\tau)\equiv-\langle T_\tau c_{\mathbf{k}\sigma}(\tau)c^\dagger_{\mathbf{k}\sigma}(0)\rangle, \tag{43}$$

$$G_{\Gamma\alpha\sigma}(\mathbf{k},\tau)\equiv-\langle T_\tau f_{\mathbf{k}\Gamma\alpha}(\tau)c^\dagger_{\mathbf{k}\sigma}(0)\rangle, \tag{44}$$

where T_τ is the imaginary time ordering operator. In terms of a complex frequency z, the mean-field Green functions are

$$G_{\Gamma\alpha\Gamma'\alpha'}(\mathbf{k},z)=\frac{1}{z-\epsilon_\Gamma}\left[\delta_{\Gamma\Gamma'}\delta_{\alpha\alpha'}+\frac{1}{z-\epsilon_{\Gamma'}}\frac{(z-\epsilon_7)(z-\epsilon_8)\tilde{s}_{0\Gamma}\tilde{V}^*_{\Gamma\alpha\sigma}(\mathbf{k})\tilde{V}_{\Gamma'\alpha'\sigma}(\mathbf{k})\tilde{s}_{0\Gamma'}}{(z-E_{1\mathbf{k}})(z-E_{2\mathbf{k}})(z-E_{3\mathbf{k}})}\right], \tag{45}$$

$$G_\sigma(\mathbf{k},z)=\frac{(z-\epsilon_7)(z-\epsilon_8)}{(z-E_{1\mathbf{k}})(z-E_{2\mathbf{k}})(z-E_{3\mathbf{k}})}, \tag{46}$$

$$G_{\Gamma\alpha\sigma}(\mathbf{k},z)=\frac{\tilde{s}_{0\Gamma}\tilde{V}^*_{\Gamma\alpha\sigma}(\mathbf{k})(z-\epsilon_{\Gamma^*})}{(z-E_{1\mathbf{k}})(z-E_{2\mathbf{k}})(z-E_{3\mathbf{k}})}. \tag{47}$$

These propagators will be used to calculate the Green functions for the bosonic fields in our Hamiltonian, namely, $\tilde{s}_{\mathbf{k}\Gamma}$ and $i\lambda_{\mathbf{k}}$. The bosonic Green functions can be dressed (through the terms $H_{\rm mix}$ and H_f) by particle-hole excitations of the hybridized conduction and $4f$ electron systems. To proceed, we write the slave boson and Lagrange multipliers as follows:

$$\tilde{s}_{\mathbf{k}\Gamma}=\tilde{s}_{0\Gamma}\delta_{\mathbf{k},0}+\delta\tilde{s}_{\mathbf{k}\Gamma}, \tag{48}$$

$$i\lambda_{\mathbf{k}}=i\lambda_0\delta_{\mathbf{k},0}+i\delta\lambda_{\mathbf{k}}, \tag{49}$$

where $\delta\tilde{s}_{\mathbf{k}\Gamma}$ and $\delta\lambda_{\mathbf{k}}$ represent fluctuations away from the (self-consistent) mean-field values.

It is easy to see how the particle-hole excitations dress the bosonic Green functions by writing the *full* Hamiltonian in k space,

$$\begin{aligned}H=&\sum_{\mathbf{k}\sigma}\xi_{\mathbf{k}}c^\dagger_{\mathbf{k}\sigma}c_{\mathbf{k}\sigma}+\sum_{\mathbf{k}\mathbf{k}'\Gamma\alpha}f^\dagger_{\mathbf{k}\Gamma\alpha}\left[E_\Gamma\delta_{\mathbf{k}\mathbf{k}'}+i\lambda_{\mathbf{k}-\mathbf{k}'}\right]f_{\mathbf{k}'\Gamma\alpha}\\&+\sum_{\mathbf{k}\mathbf{k}'\Gamma\alpha\sigma}\left[\tilde{V}_{\Gamma\alpha\sigma}(\mathbf{k})c^\dagger_{\mathbf{k}\sigma}f_{\mathbf{k}'\Gamma\alpha}\tilde{s}^*_{\mathbf{k}'-\mathbf{k}\Gamma}+\text{H.c.}\right]\\&+\frac{N_s}{2}\sum_{\mathbf{k}\Gamma}N_\Gamma i\lambda_{\mathbf{k}}\left[\sum_{\mathbf{k}'}\tilde{s}^*_{\mathbf{k}+\mathbf{k}'\Gamma}\tilde{s}_{\mathbf{k}\Gamma}-q_\Gamma\right].\end{aligned} \tag{50}$$

Substituting from Eqs. (48) and (49), Eq. (50) can be written in two pieces, one representing the mean-field approximation (which we have solved), and the second piece coming from the fluctuations in the bosonic fields $\delta\tilde{s}_{\mathbf{k}\Gamma}$ and $\delta\lambda_{\mathbf{k}}$. The *bare* boson Green functions come from the terms in the constraint, the last line of Eq. (50), which are quadratic in the fluctuating fields. Since this involves

terms of the form $\delta\tilde{s}_{\mathbf{k}\Gamma}\delta\tilde{s}_{\mathbf{k}\Gamma}$, $\delta\tilde{s}_{\mathbf{k}\Gamma}\delta\lambda_{\mathbf{k}}$, and $\delta\lambda_{\mathbf{k}}\delta\lambda_{\mathbf{k}}$, we write the bare propagator in a matrix form (in the static limit),

$$\hat{D}^{-1}_{0\Gamma\Gamma'} = -\frac{N_\Gamma}{2}\begin{pmatrix} i\lambda_0 & \tilde{s}_{0\Gamma} \\ \tilde{s}_{0\Gamma} & 0 \end{pmatrix}\delta_{\Gamma\Gamma'}, \tag{51}$$

where $\tilde{s}_{0\Gamma} = s_0/\sqrt{N_\Gamma}$. The specific elements of the matrix are $D_{0ss\Gamma\Gamma'} = -\frac{N_\Gamma}{2}i\lambda_0\delta_{\Gamma\Gamma'}$, $D_{0s\lambda\Gamma\Gamma'} = -\frac{N_\Gamma}{2}\tilde{s}_{0\Gamma}\delta_{\Gamma\Gamma'}$, and $D_{0\lambda\lambda\Gamma\Gamma'}=0$.

The *dressed* boson Green function will then satisfy a matrix Dyson's equation,

$$\hat{D}^{-1}_{\Gamma\Gamma'}(\mathbf{q}) = \hat{D}^{-1}_{0\Gamma\Gamma'}(\mathbf{q}) - \hat{\Pi}_{\Gamma\Gamma'}(\mathbf{q}). \tag{52}$$

The 2×2 self-energy matrix $\hat{\Pi}_{\Gamma\Gamma'}(\mathbf{q})$, due to the particle-hole excitations (one-loop order), can be calculated by the usual Feynman diagrammatic techniques.

Figure 4 shows all the unique self-energy diagrams in terms of the three hybridization-dressed fermionic Green functions, Eqs. (42)–(44). Evaluation of theses diagrams leads to the following results for the elements of the (inverse) dressed Bose propagator:

$$D^{-1}_{ss\Gamma\Gamma'}(\mathbf{q}) = 2I_{ss\Gamma\Gamma'}(\mathbf{q}), \tag{53}$$

$$D^{-1}_{s\lambda\Gamma\Gamma'} = -i\left[\frac{N_\Gamma}{2}\tilde{s}_{0\Gamma} + \frac{x_\Gamma}{\tilde{s}_{0\Gamma}}\right]\delta_{\Gamma\Gamma'} + iI_{s\lambda\Gamma\Gamma'}(\mathbf{q}), \tag{54}$$

$$D^{-1}_{\lambda\lambda\Gamma\Gamma'}(\mathbf{q}) = -\frac{y_\Gamma}{T_{0\Gamma}} - \frac{1}{2}I_{\lambda\lambda\Gamma\Gamma'}(\mathbf{q}), \tag{55}$$

where the momentum dependent functions are given by

$$I_{ss\Gamma\Gamma'}(\mathbf{q}) \equiv \frac{P}{N_s}\sum_{\mathbf{k}\mathbf{k}'\alpha\alpha'} \frac{f(E_{1\mathbf{k}})\tilde{s}_{0\Gamma}\tilde{s}_{0\Gamma'}\mu_{\Gamma\alpha\Gamma'\alpha'}(\mathbf{k})\mu_{\Gamma'\alpha'\Gamma\alpha}(\mathbf{k}')(\epsilon_7 - E_{1\mathbf{k}})^2(\epsilon_8 - E_{1\mathbf{k}})^2}{(E_{1\mathbf{k}'} - E_{1\mathbf{k}})(E_{2\mathbf{k}'} - E_{1\mathbf{k}})(E_{3\mathbf{k}'} - E_{1\mathbf{k}})(E_{2\mathbf{k}} - E_{1\mathbf{k}})} \frac{[\delta_{\mathbf{k}',\mathbf{k}+\mathbf{q}} + \delta_{\mathbf{k}',\mathbf{k}-\mathbf{q}}]}{(\epsilon_\Gamma - E_{1\mathbf{k}})(\epsilon_{\Gamma'} - E_{1\mathbf{k}})(E_{3\mathbf{k}} - E_{1\mathbf{k}})}, \tag{56}$$

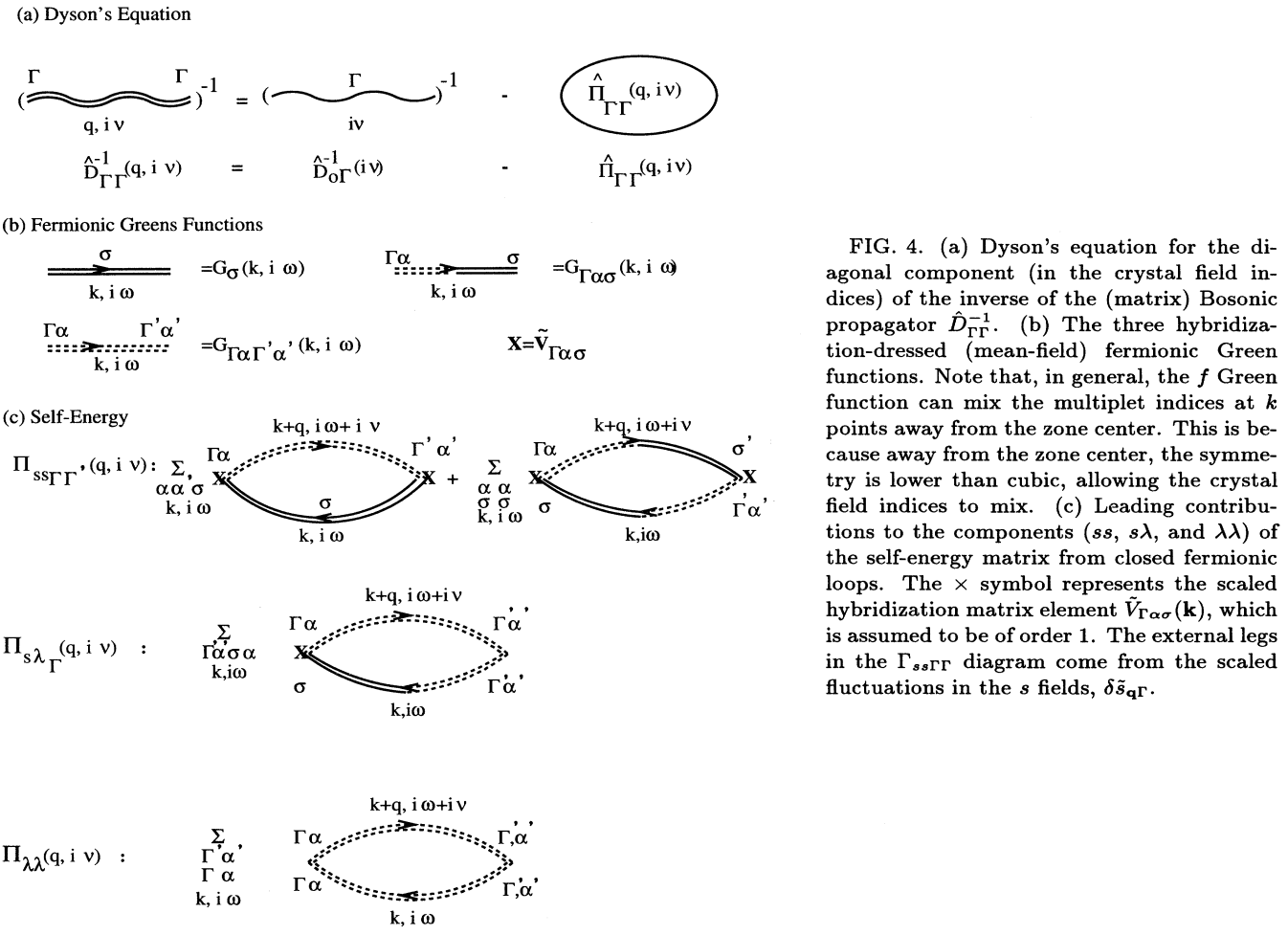

FIG. 4. (a) Dyson's equation for the diagonal component (in the crystal field indices) of the inverse of the (matrix) Bosonic propagator $\hat{D}^{-1}_{\Gamma\Gamma}$. (b) The three hybridization-dressed (mean-field) fermionic Green functions. Note that, in general, the f Green function can mix the multiplet indices at k points away from the zone center. This is because away from the zone center, the symmetry is lower than cubic, allowing the crystal field indices to mix. (c) Leading contributions to the components (ss, $s\lambda$, and $\lambda\lambda$) of the self-energy matrix from closed fermionic loops. The $\times$ symbol represents the scaled hybridization matrix element $\tilde{V}_{\Gamma\alpha\sigma}(\mathbf{k})$, which is assumed to be of order 1. The external legs in the $\Gamma_{ss\Gamma\Gamma}$ diagram come from the scaled fluctuations in the s fields, $\delta\tilde{s}_{\mathbf{q}\Gamma}$.

$$I_{s\lambda\Gamma\Gamma'}(\mathbf{q}) \equiv \frac{P}{N_s}\sum_{\mathbf{k}\mathbf{k}'}\frac{f(E_{1\mathbf{k}})(\epsilon_7-E_{1\mathbf{k}})^2(\epsilon_8-E_{1\mathbf{k}})^2}{(E_{2\mathbf{k}}-E_{1\mathbf{k}})(E_{3\mathbf{k}}-E_{1\mathbf{k}})(E_{1\mathbf{k}'}-E_{1\mathbf{k}})(E_{2\mathbf{k}'}-E_{1\mathbf{k}})(E_{3\mathbf{k}'}-E_{1\mathbf{k}})}$$
$$\times\sum_{\alpha\alpha'}\frac{\tilde{s}_{0\Gamma}\tilde{s}_{0\Gamma'}}{(E_{1\mathbf{k}}-\epsilon_\Gamma)(E_{1\mathbf{k}}-\epsilon_{\Gamma'})}\left[\frac{\tilde{s}_{0\Gamma}\mu_{\Gamma\alpha\Gamma'\alpha'}(\mathbf{k})\mu_{\Gamma'\alpha'\Gamma\alpha}(\mathbf{k}')}{(E_{1\mathbf{k}}-\epsilon_\Gamma)}+\frac{\tilde{s}_{0\Gamma'}\mu_{\Gamma'\alpha'\Gamma\alpha}(\mathbf{k})\mu_{\Gamma\alpha\Gamma'\alpha'}(\mathbf{k}')}{(E_{1\mathbf{k}}-\epsilon_{\Gamma'})}\right]\left[\delta_{\mathbf{k}',\mathbf{k}+\mathbf{q}}+\delta_{\mathbf{k}',\mathbf{k}-\mathbf{q}}\right], \tag{57}$$

$$I_{\lambda\lambda\Gamma\Gamma'}(\mathbf{q}) \equiv \frac{P}{N_s}\sum_{\mathbf{k}\mathbf{k}'\alpha\alpha'}\frac{f(E_{1\mathbf{k}})\tilde{s}^2_{0\Gamma}\tilde{s}^2_{0\Gamma'}\mu_{\Gamma\alpha\Gamma'\alpha'}(\mathbf{k}')\mu_{\Gamma'\alpha'\Gamma\alpha}(\mathbf{k})\left[\delta_{\mathbf{k}',\mathbf{k}-\mathbf{q}}+\delta_{\mathbf{k}',\mathbf{k}+\mathbf{q}}\right]}{(E_{1\mathbf{k}'}-E_{1\mathbf{k}})(E_{2\mathbf{k}'}-E_{1\mathbf{k}})(E_{3\mathbf{k}'}-E_{1\mathbf{k}})(E_{2\mathbf{k}}-E_{1\mathbf{k}})}\frac{(\epsilon_7-E_{1\mathbf{k}})^2(\epsilon_8-E_{1\mathbf{k}})^2}{(\epsilon_\Gamma-E_{1\mathbf{k}})^2(\epsilon_{\Gamma'}-E_{1\mathbf{k}})^2(E_{3\mathbf{k}}-E_{1\mathbf{k}})}. \tag{58}$$

In Eqs. (56)–(58), $E_{n\mathbf{k}}$ are the quasiparticle band energies. The quasiparticle chemical potential was chosen to lie in the lowest band, such that $f(E_{n\mathbf{k}})$ is nonzero only for $n = 1$. (Recall this is a zero temperature calculation.) The anisotropic function $\mu_{\Gamma\alpha\Gamma'\alpha'}(\mathbf{k})$ is defined in Eq. (17). The parameters x_Γ and y_Γ are numbers which depend on the mean-field parameter set used. See Table IV for the values of these parameters.

We must evaluate numerically the three-dimensional principal value integrals comprising the functions $I_{ss\Gamma\Gamma'}(\mathbf{q})$, $I_{s\lambda\Gamma\Gamma'}(\mathbf{q})$, and $I_{\lambda\lambda\Gamma\Gamma'}(\mathbf{q})$ of Eqs. (56)–(58). To do so, we use a procedure developed originally to calculate the real part of spectral functions of the form,[38–41]

$$\Phi'(E) = \mathrm{Re}\Phi(E) = P\frac{1}{N_s}\sum_{\mathbf{k}}\frac{M(\mathbf{k})}{E-E_{n\mathbf{k}}}. \tag{59}$$

Φ' looks like the real part of a dynamic susceptibility. We write our functions $I_{ab\Gamma\Gamma'}(\mathbf{q})$ in the following form:

$$I_{ab\Gamma\Gamma'}(\mathbf{q}) = \frac{P}{N_s}\sum_{\mathbf{k}\mathbf{k}'}\frac{f(E_{1\mathbf{k}})M_{ab\Gamma\Gamma'}(\mathbf{k},\mathbf{k}')}{E_{1\mathbf{k}'}-E_{1\mathbf{k}}}\delta_{\mathbf{k}',\mathbf{k}\pm\mathbf{q}}, \tag{60}$$

where the matrix elements are a complicated function of $\mathbf{k}$ and $\mathbf{q}$ which come from Eqs. (56), (57), and (58). That is, direct comparison of Eq. (60) with Eqs. (56)–(58) gives the structure of the matrix elements $M_{ab\Gamma\Gamma'}\mathbf{k},\mathbf{k}'$. Note that the symbols ab can represent ss, $s\lambda$, or $\lambda\lambda$.

Note that these three-dimensional integrals can have an entire surface of poles inside the Brillouin zone that must be handled properly. In contrast, a one-dimensional principal value integral can be regularized numerically by basically subtracting off the divergence,[42] and such a procedure is facilitated by the relatively small number of poles throughout the domain of integration. In our three-dimensional integral, if n^3_{mesh} is the number of cubes into which the Brillouin zone is divided for the purpose of numerical integration, then there are of the order of n^2_{mesh} poles, which clearly gets large as n_{mesh} increases, and it is no longer possible to regularize the integral in a simple way. The large quantity of work done by (mostly electronic structure) physicists in this field of numerical k-space sums is indicative of the degree of complexity inherent to these problems.[43,44]

We now show the dependence of the self-energy function $I_{ss}(\mathbf{q})$, which has been summed over the crystal field multiplet indices,

$$I_{ss}(\mathbf{q}) \equiv \sum_{\Gamma\Gamma'}\frac{I_{ss\Gamma\Gamma'}(\mathbf{q})}{\sqrt{N_\Gamma}\sqrt{N_{\Gamma'}}}, \tag{61}$$

as a function of n_{mesh}. Within our implementation of the analytic tetrahedron method, for a given mesh parameter n_{mesh}, the total number of tetrahedra in the Brillouin zone is $8n^3_{\mathrm{mesh}}$. The function I_{ss} is plotted as a function of the mesh parameter n_{mesh} in Fig. 5 for mean-field parameter set (a). The results for parameter set (b) are similar. We chose the momentum $q = 0.5\hat{z}$, measured in units of π/a, where a is the lattice spacing. (We took a =3.89 Å.) The matrix elements are assumed constant inside a given tetrahedron. Since they are complicated anisotropic functions, however, the matrix elements can vary a great deal throughout the Brillouin zone, and thus they cause fluctuations in the value of the $I_{ss}(\mathbf{q})$ as a function of n_{mesh}. This is clearly visible in Fig. 5 for the case of $I_{ss}(\mathbf{q})$. The behavior of $I_{s\lambda}(\mathbf{q})$ and $I_{\lambda\lambda}(\mathbf{q})$ is qualitatively similar.

It is clear that if we need convergence of the Green

TABLE IV. The parameters x_Γ and y_Γ are for both mean-field parameter sets described in Table II.

Parameter set	x_7	x_8	y_7	y_8
(a)	1.820	0.0717	0.975	0.04029
(b)	1.729	0.0949	0.925	0.0498

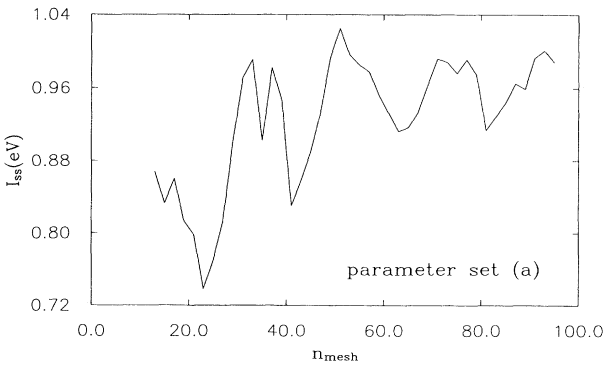

FIG. 5. Numerically evaluated function $I_{ss}(\mathbf{q})$ as a function of the mesh parameter n_{mesh} for mean-field parameter set (a). Here we used $\mathbf{q} = 0.5\hat{z}$.

functions to several decimal places, it would require a mesh with $n_{\rm mesh} > 80$. In background, a calculation for $n_{\rm mesh} = 40$ takes about 1 h on a DEC 5100. Since the computing time goes as $n_{\rm mesh}^3$, it is clear that a run with $n_{\rm mesh} = 80$ requires a long run time. Actually, this numerical integration is parallel in nature. Each of the $n_{\rm mesh}^3$ subcubes could, in principle, be integrated independently of the others, and at the end the net result would be the sum of the results from each subcube. Naively, this is the kind of problem a parallel machine should be able to handle well.

It is also interesting to note that calculations of the susceptibility or dielectric function based on electronic structure data, generally, are not performed for $n_{\rm mesh}$ greater than about 30.[45] The complicated nature of our matrix elements has forced us to push the procedure to very large values (by anyone's standards) of $n_{\rm mesh}$. We shall discuss in the next section how our conclusions on pairing instabilities in the infinite-U Anderson lattice take into account this slow convergence of the bosonic self-energy.

VI. QUASIPARTICLE SCATTERING AMPLITUDE

In this section, we present our analysis of the scattering amplitude $\Gamma_{\rm QP}(\mathbf{k},\mathbf{k}')$, which allows for quasiparticle interactions via the exchange of $4f$ density fluctuations. The exchanged boson will be represented by the (dressed to order 1/N) boson matrix Green function calculated in Sec. V. The diagrams for the scattering amplitude are presented in Fig. 6, where the straight lines represent the incoming (and outgoing) quasiparticles and the wavy line is an element of the (matrix) boson Green function $\hat{D}_{\Gamma\Gamma'}(\mathbf{q})$. The large black circles represent quasiparticle vertices $\gamma_{f\Gamma}(\mathbf{k},\mathbf{k}')$ and $\gamma_{{\rm mix}\Gamma}(\mathbf{k},\mathbf{k}')$, which are calculated by writing the full Hamiltonian in the quasiparticle basis:

$$H_{\rm QP} = \sum_{\mathbf{k}\sigma nn'} \xi_{\mathbf{k}} A_n^*(\mathbf{k}) A_{n'}(\mathbf{k}) Q^\dagger_{\mathbf{k}n\sigma} Q_{\mathbf{k}n'\sigma} + \sum_{\mathbf{k}\mathbf{k}'\Gamma\alpha nn'\sigma\sigma'} \gamma_{f\Gamma}(\mathbf{k},\mathbf{k}') Q^\dagger_{\mathbf{k}n\sigma} \left[E_\Gamma \delta_{\mathbf{k}\mathbf{k}'} + i\lambda_{\mathbf{k}-\mathbf{k}'} \right] Q_{\mathbf{k}'n'\sigma'}$$
$$+ \sum_{\mathbf{k}\mathbf{k}'\Gamma\alpha\sigma nn'\sigma'} \left[\gamma_{{\rm mix}\Gamma}(\mathbf{k},\mathbf{k}') Q^\dagger_{\mathbf{k}n\sigma} Q_{\mathbf{k}'n'\sigma'} \tilde{s}^*_{\mathbf{k}'-\mathbf{k}\Gamma} + {\rm H.c.} \right] + H_{\rm constraint}. \tag{62}$$

Recall that $Q_{\mathbf{k}n\sigma}$ destroys a quasiparticle of momentum $\mathbf{k}$, pseudospin σ, and band index n. The vertex functions γ_f and $\gamma_{\rm mix}$ thus come from the unitary transformation that diagonalizes $H_{\rm MF}$ [see Eqs. (19) and (20)],

$$\gamma_{f\Gamma}(\mathbf{k},\mathbf{k}') \equiv \frac{A_n^*(\mathbf{k}) A_{n'}(\mathbf{k}') \tilde{s}_{0\Gamma}^2 \tilde{V}^*_{\Gamma\alpha\sigma'}(\mathbf{k}') \tilde{V}_{\sigma\Gamma\alpha}(\mathbf{k})}{(\epsilon_\Gamma - E_{n\mathbf{k}})(\epsilon_\Gamma - E_{n'\mathbf{k}'})}, \tag{63}$$

$$\gamma_{{\rm mix}\Gamma}(\mathbf{k},\mathbf{k}') \equiv -\frac{A_n^*(\mathbf{k}) A_{n'}(\mathbf{k}') \tilde{s}_{0\Gamma} \tilde{V}^*_{\Gamma\alpha\sigma'}(\mathbf{k}') \tilde{V}_{\Gamma\alpha\sigma}(\mathbf{k})}{\epsilon_\Gamma - E_{n'\mathbf{k}'}}. \tag{64}$$

As shown below, we project $\Gamma_{\rm QP}(\mathbf{k},\mathbf{k}')$ onto states of cubic symmetry, $\Phi_\eta(\mathbf{k})$, the so-called cubic harmonics, where η labels the irreducible representations of the octahedral group $\mathcal{O}_h$. The product is then averaged over the Fermi surface,

$$\Gamma_\eta = \int \frac{d\hat{k}}{4\pi} \int \frac{d\hat{k}'}{4\pi} \Phi^*_\eta(\hat{k}') \Gamma_{\rm QP}(\mathbf{k},\mathbf{k}') \Phi_\eta(\hat{k}). \tag{65}$$

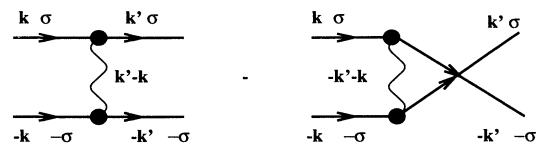

FIG. 6. Quasiparticle scattering amplitude for incoming particles (solid lines) of momenta $\mathbf{k}$ and $-\mathbf{k}$. The wavy lines are dressed boson propagators, and the vertices denote the anisotropic coupling of quasiparticles to bosons.

A superconducting instability of symmetry η is signaled by a negative value of the corresponding average Γ_η. See Table V for a list of the cubic harmonics used in this calculation. The character table for the octahedral group $\mathcal{O}$ is presented in Table VI, where the irreducible representations are listed: A_1, A_2, E, T_1, and T_2. The group $\mathcal{O}_h$ follows from the group $\mathcal{O}$ by including inversions. This means the representations pick up a subscript g or u depending on if they are even or odd, respectively, under parity. Because of the complexity in calculating the dressed Bose propagators, we have assumed a spherical Fermi surface for the average in Eq. (65). We do not feel this is a weakness of the calculation for reasons discussed

TABLE V. Realizations of the cubic harmonics Φ_η as linear combinations of the spherical harmonics Y_{lm}. For each representation η of cubic symmetry, the expansion was cut off after the lowest set of spherical harmonics with $l > 0$.

η	Φ_η
A_{1g}	$\frac{1}{\sqrt{2}}\left(Y_{00} + 0.76376261 Y_{40} + 0.4564355(Y_{44} + Y_{4-4})\right)$
A_{2g}	$0.58630197(Y_{62} + Y_{6-2}) - 0.3952847(Y_{66} + Y_{6-6})$
E_g	Y_{20}
E_g	$\frac{1}{\sqrt{2}}(Y_{22} + Y_{2-2})$
T_{1g}	$\left(\frac{-0.93541435i}{\sqrt{2}}(Y_{41} - Y_{4-1}) - \frac{0.353553391i}{\sqrt{2}}(Y_{43} - Y_{4-3})\right)$
T_{1g}	$\left(\frac{0.93541435}{\sqrt{2}}(Y_{41} + Y_{4-1}) - \frac{-0.353553391}{\sqrt{2}}(Y_{43} + Y_{4-3})\right)$
T_{1g}	$\frac{i}{\sqrt{2}}(Y_{44} - Y_{4-4})$
T_{2g}	$\frac{i}{\sqrt{2}}(Y_{21} - Y_{2-1})$
T_{2g}	$\frac{1}{\sqrt{2}}(Y_{21} + Y_{2-1})$
T_{2g}	$\frac{i}{\sqrt{2}}(Y_{22} - Y_{2-2})$

TABLE VI. Irreducible representations of the octahedral group O. To get the group O_h, we add inversions to the allowed symmetry operations, the result of which is that all representations pick up a subscript g (for even parity) or u (for odd parity).

Representation	Dimensionality	Transforms like
A_1	1	$x^2+y^2+z^2$
A_2	1	$(x^2-y^2)(z^2-x^2)(y^2-z^2)$
E	2	$x^2-y^2, 3z^2-r^2$
T_1	3	x, y, z
T_2	3	xy, yz, zx

elsewhere.[22]

In this paper, we shall consider only even-parity pairing states. This restriction is based on the following experimental evidence for $CeCu_2Si_2$: the need for strong Pauli limiting to fit the low-temperature upper critical field data $H_{c2}(0)$,[25] the reduced spin susceptibility below T_c as measured by the ^{63}Cu Knight shift,[46] and the observed T^3 temperature dependence of the nuclear-spin relaxation rate below T_c.[46] The strong Pauli limiting actually only argues against equal spin pairing states. As Ueda and Rice showed,[47] in the presence of spin-orbit coupling, Pauli limiting is possible for pairing states of T_{1u} or T_{2u} symmetry. (Both of these odd-parity states would have a gap with point nodes as opposed to line nodes on the Fermi surface.) These experimental facts put together, however, might be considered reasonable evidence for even-parity pairing in $CeCu_2Si_2$.

We have found it useful to study the properties of the scattering amplitude in two steps. First, by setting the functions $I_{ss\Gamma\Gamma'}(\mathbf{q})$, $I_{s\lambda\Gamma\Gamma'}(\mathbf{q})$, and $I_{\lambda\lambda\Gamma\Gamma'}(\mathbf{q})$ to zero, we simplify the problem considerably to that of two quasiparticles scattering via exchange of a momentum independent boson. In real space, this corresponds to a local interaction between the quasiparticles. We find that these local interactions, when averaged over the Fermi surface, are substantially different from those calculated within the jellium model by Zhang and Lee.[17]

In the case of cubic symmetry, inclusion of the functions $I_{ss\Gamma\Gamma'}(\mathbf{q})$, $I_{s\lambda\Gamma\Gamma'}(\mathbf{q})$, and $I_{\lambda\lambda\Gamma\Gamma'}(\mathbf{q})$ is the computationally intensive part of this calculation. If there are strong local *repulsive* interactions in the η pairing channel, then the only way to get a pairing instability (i.e., $\Gamma_\eta<0$) is to have the functions $I_{ss\Gamma\Gamma'}(\mathbf{q})$, $I_{s\lambda\Gamma\Gamma'}(\mathbf{q})$, and $I_{\lambda\lambda\Gamma\Gamma'}(\mathbf{q})$, which represent the effect of nonlocal interactions, overcome the repulsion. Zhang and Lee discovered that in the jellium model these q-dependent contributions are too weak to overcome the local repulsions in the s-, d-, and g-wave pairing states. We find that in cubic symmetry (with crystal field splitting) attractive nonlocal interactions can overpower local repulsions in the T_{1g} pairing channel, thus giving evidence for a T_{1g} pairing instability.

When we evaluate the diagrams of Fig. 6, we can write the quasiparticle scattering amplitude in the even-parity (pseudospin singlet) channel as

$$\begin{aligned}\Gamma_{QP}(\mathbf{k},\mathbf{k}') = \frac{1}{4}\sum_{\Gamma\alpha\Gamma'\alpha'\sigma\sigma'} & \frac{A_1^2(\mathbf{k})A_1^2(\mathbf{k}')\tilde{s}_{0\Gamma}\tilde{s}_{0\Gamma'}\tilde{V}^*_{\Gamma\alpha\sigma'}(\mathbf{k}')\tilde{V}_{\sigma'\Gamma'\alpha'}(\mathbf{k}')\tilde{V}^*_{\Gamma'\alpha'\sigma}(\mathbf{k})\tilde{V}_{\sigma\Gamma\alpha}(\mathbf{k})}{(\epsilon_\Gamma-E_{1\mathbf{k}})(\epsilon_{\Gamma'}-E_{1\mathbf{k}})} \\ \times\Bigg[& D_{ss\Gamma\Gamma'}(\mathbf{k}'-\mathbf{k})+D_{ss\Gamma\Gamma'}(-\mathbf{k}'-\mathbf{k})-i\frac{\tilde{s}_{0\Gamma}}{\epsilon_\Gamma-E_{1\mathbf{k}'}}\Big(D_{s\lambda\Gamma'}(\mathbf{k}'-\mathbf{k})+D_{s\lambda\Gamma'}(-\mathbf{k}'-\mathbf{k})\Big) \\ & -i\frac{\tilde{s}_{0\Gamma'}}{\epsilon_{\Gamma'}-E_{1\mathbf{k}'}}\Big(D_{s\lambda\Gamma}(\mathbf{k}'-\mathbf{k})+D_{s\lambda\Gamma}(-\mathbf{k}'-\mathbf{k}')\Big) \\ & -\frac{\tilde{s}_{0\Gamma}\tilde{s}_{0\Gamma'}}{(\epsilon_\Gamma-E_{1\mathbf{k}'})(\epsilon_{\Gamma'}-E_{1\mathbf{k}'})}\Big(D_{\lambda\lambda}(\mathbf{k}'-\mathbf{k})+D_{\lambda\lambda}(-\mathbf{k}'-\mathbf{k})\Big)\Bigg],\end{aligned} \tag{66}$$

where the components of the bosonic Green function are

$$D_{ss\Gamma\Gamma'}(\mathbf{q},\tau)\equiv\langle\delta\tilde{s}_{-\mathbf{q}\Gamma}(\tau)\delta\tilde{s}_{\mathbf{q}\Gamma'}(0)\rangle,$$

$$D_{s\lambda\Gamma}(\mathbf{q},\tau)\equiv\langle\delta\tilde{s}_{-\mathbf{q}\Gamma}(\tau)\delta\lambda_{\mathbf{q}}(0)\rangle,$$

$$D_{\lambda\lambda}(\mathbf{q},\tau)\equiv\langle\delta\lambda_{-\mathbf{q}}(\tau)\delta\lambda_{\mathbf{q}}(0)\rangle,$$

and all other symbols have been previously defined. Note that we are taking the static limit of these Green functions. We are limiting ourselves to a Fermi surface average of the scattering amplitude, that is, a weak-coupling calculation. It became clear that including the frequency dependence of the boson Green functions was impossible, given the difficult numerical integrals encountered even in the static limit.

When evaluated on the Fermi surface (at zero temperature), the band energies $E_{1\mathbf{k}}$ and $E_{1\mathbf{k}'}$ are set equal to the quasiparticle chemical potential μ. Thus a term like $\epsilon_\Gamma-E_{1\mathbf{k}}$ becomes

$$\epsilon_\Gamma-\mu=T_{0\Gamma}, \tag{67}$$

which is the Kondo temperature of the Γ multiplet. For the case of $CeCu_2Si_2$, the Kondo temperature of the Γ_7 doublet is approximately 10 K, while for the Γ_8 quartet $T_{08}=T_{07}+\Delta_{CEF}=370$ K. This explains how to treat all the energy denominators in Eq. (66).

As mentioned, it is instructive to consider the so-called local limit of Eq. (66) in which the self-energy functions $I_{ss}(\mathbf{q})$, $I_{s\lambda}(\mathbf{q})$, and $I_{\lambda\lambda}(\mathbf{q})$ are set to zero,

$$\Gamma_{\rm local}(\mathbf{k},\mathbf{k}') = \frac{1}{4}\sum_{\Gamma\alpha\Gamma'\alpha'\sigma\sigma'} \frac{A_1^2(\mathbf{k})A_1^2(\mathbf{k}')\tilde{s}_{0\Gamma}\tilde{s}_{0\Gamma'}\tilde{V}^*_{\Gamma\alpha\sigma}(\mathbf{k}')\tilde{V}_{\sigma'\Gamma'\alpha'}(\mathbf{k}')\tilde{V}^*_{\Gamma'\alpha'\sigma}(\mathbf{k})\tilde{V}_{\sigma\Gamma\alpha}(\mathbf{k})}{T_{0\Gamma}T_{0\Gamma'}} \times 2\left[\frac{\tilde{s}_{0\Gamma}}{\sqrt{N_{\Gamma'}}T_{0\Gamma}\Gamma_{0s\lambda}} + \frac{\tilde{s}_{0\Gamma'}}{\sqrt{N_{\Gamma}}T_{0\Gamma'}\Gamma_{0s\lambda}} - \frac{\Gamma_{0\lambda\lambda}}{\sqrt{N_{\Gamma}N_{\Gamma'}}\Gamma^2_{0s\lambda}}\right], \tag{68}$$

where

$$\Gamma_{0s\lambda} = \sum_{\Gamma}\left(\frac{1}{2}N_{\Gamma}\tilde{s}_{0\Gamma} + \frac{x_{\Gamma}}{\tilde{s}_{0\Gamma}}\right), \tag{69}$$

$$\Gamma_{0\lambda\lambda} = \sum_{\Gamma}\frac{y_{\Gamma}}{T_{0\Gamma}}. \tag{70}$$

The combination of normalization functions $A_1^2(\mathbf{k})A_1^2(\mathbf{k}')$ and the product of the four hybridization matrix elements is due to the anisotropic vertices $\gamma_{\rm mix\Gamma}(\mathbf{k},\mathbf{k}')$ and $\gamma_{f\Gamma'}(\mathbf{k},\mathbf{k}')$. The contribution from the Bose Green function is that which remains inside the square brackets in Eq. (68).

The local scattering amplitude of Eq. (68) is much simpler to deal with than the full expression of Eq. (66). Roughly, the functions $I_{ss}(\mathbf{q})$, $I_{s\lambda}(\mathbf{q})$, and $I_{\lambda\lambda}(\mathbf{q})$ can be thought of as renormalizing the local interactions. In the next two sections, we present our results for the Fermi-surface-averaged scattering amplitude Γ_η, both with and without the bosonic self-energy.

VII. RESULTS: LOCAL LIMIT

We now present our results for the Fermi-surface-averaged (local) quasiparticle interactions $\Gamma_{{\rm local},\eta}$, where η=A_{1g}, E_g, T_{1g}, or T_{2g}. We have not included pairing states in the A_{2g} representation (see Tables V and VI) for two reasons: (1) The lowest-order spherical harmonic present in the cubic harmonic $\Phi_{A_{2g}}$ is Y_{6m},[48] and the relatively rapid variation throughout the Brillouin zone of the pair wave function would correspond to a pairing state with a high kinetic energy and hence should be less accessible than the pairing states labeled by the other representations; (2) the A_{2g} state would also require a finer mesh for the Fermi surface average than the one we have used and hence would further increase the (already considerable) overall computing time.

Table VII gives the ratio $\Gamma_{{\rm local},\eta}/T_{07}$ for both mean-field parameter sets (a) and (b). Also presented in Table VII is the contribution to the Fermi surface average from the so-called hot spots. For the hot spot contribution, the normalization functions $A_1^2(\mathbf{k})$ and $A_1^2(\mathbf{k}')$ in Eq. (68) were approximated with δ functions in k space that sampled only the six points on the Fermi surface intersected by the Brillouin zone axes. The integrated weight of the δ functions was chosen to equal the area under the peaks, as shown in Fig. 2. Such a calculation gives us a feeling for the importance of these special points where the normalization function $A_1(\mathbf{k})$ is rapidly changing. This contribution is labeled by $\Gamma_{\rm local,hot}$ in Table VII. We see the following.

(i) The A_{1g} pairing channel has (by far) the largest (repulsive) local interaction, but it is not dominated by what happens at the hot spots.

(ii) In the E_g channel, the strong anisotropy of the normalization function gives rise to a weakly *attractive* local interaction. In fact, the attractive local interaction here is dominated by the contributions from the hot spots. Note from Table VI that a pairing state of E_g symmetry

TABLE VII. The local ("hard-core") quasiparticle scattering amplitude in the presence of crystal electric fields, $\Gamma_{\rm QP}$, averaged over a spherical Fermi surface. Results for both mean-field parameter sets (a) and (b) are given. See Table III for a discussion of the mean-field parameters themselves. The first column gives the representations, labeled by η, of the group O_h. The second and third columns are the averaged local scattering amplitudes (divided by the Γ_7 Kondo temperature T_{07}) for the parameter sets (a) and (b), respectively. The fourth column lists [for parameter set (a)] the contribution to the average from the so-called hot spots, where the Brillouin zone axes intersect the Fermi surface. In column 4, in the E_g channel, the attractive interaction seems to be due to these hot spots; but in the A_{1g} channel the hot spots do not dominate, since the full Fermi surface average is large and positive. The average in the E_g *should* be most sensitive to the hot spots, since that is where the E_g cubic harmonics have their maximum value. In the T_{1g} and T_{2g} channels there is rigorously zero contribution from the hot spots because the T_{1g} and T_{2g} cubic harmonics vanish at those points.

(a) Cubic symmetry η	$\langle\Gamma_{\rm local}\rangle_\eta/T_{07}$ set (a)	$\langle\Gamma_{\rm local}\rangle_\eta/T_{07}$ set (b)	$\langle\Gamma_{\rm local,hot}\rangle/T_{07}$ set (a)
A_{1g}(s wave)	3.54	3.53	-0.215
$E_g(d_{x^2-y^2}, d_{3z^2-r^2})$	-0.0275	-0.0453	-0.0696
T_{1g}	0.0478	0.0695	0.0
$T_{2g}(d_{xy}, d_{yz}, d_{xz})$	0.0487	0.0709	0.0

TABLE VIII. The local ("hard-core") quasiparticle scattering amplitude in the jellium model, as studied by Zhang and Lee (Ref. 1). When divided by the Kondo temperature and averaged over the spherical Fermi surface, these results are *universal*; there are no other parameters involved. In spherical symmetry, the pairing states are labeled by their relative angular momentum l, with l=0 corresponding the s wave; l=2, d wave; and l=4, g wave. It is meaningful to compare Zhang and Lee's results with ours, because in the limit of spherical symmetry, where all the bosonic propagators in Eq. (68) are replaced with their values in spherical symmetry, and where the normalization functions $A_1^2(\mathbf{k})$ and $A_1^2(\mathbf{k}')$ are replaced by their isotropic values, our expression for $\Gamma_{\rm local}$ gives exactly the same local interactions as Zhang and Lee. Note that all local interactions are *repulsive* in spherical symmetry.

Spherical symmetry	$\langle\Gamma_{\rm local}\rangle_\eta/T_0$
η=0 (s wave)	1/3
η=2 (d wave)	8/21
η=4 (g wave)	2/7

transforms like x^2-y^2 or $3z^2-r^2$, which have maxima along the directions of the axes. The normalization is also *strongly* peaked along the axes. Thus the E_g states, of all the pairing states, are most strongly affected by the hot spots.

(iii) In the T_{1g} and T_{2g} channels, the local interaction is weak and repulsive. Neither pairing channel can "see" what happens at the hot spots, because both cubic harmonics Φ_{T1g} and Φ_{T2g} vanish identically at these points.

In Table VIII we present for comparison the results for the Fermi-surface-averaged scattering amplitude from Zhang and Lee's[17] jellium model calculation, where Legendre polynomials (P_η) play the role of the cubic harmonics. States described by η=0 are s wave, η=2 corresponds to d wave, and η=4 is g wave. Zhang and Lee find that all nonzero interactions are repulsive and of about the same strength. As we have said, they also found that the inclusion of nonlocal interactions was not sufficient to overcome the local repulsions. In cubic symmetry, however, the very weak local interactions in the E_g, T_{1g}, and T_{2g} pairing channels make a superconducing instability likely.

Detalied study of Eq. (68) has shown[49] that the dominant contribution to the local amplitude is due to the Γ_7 states. Because of the crystal field splitting, the contribution from Γ_8 states will be reduced in comparison to the contribution from the Γ_7 states by an amount of either T_{07}/T_{08} or $(T_{07}/T_{08})^2$, where for $CeCu_2Si_2$ $T_{07}/T_{08}\approx 0.03$. As discussed elsewhere,[22] if *only* the Γ_7 states were to contribute to the local amplitude, then all projections of the scattering amplitude $\Gamma_{{\rm local},\eta}$ would be zero except for $\eta=A_{1g}$. The presence of the nonzero but *weak* local interactions in the E_g, T_{1g}, and T_{2g} channels is thus mainly an effect of the excited crystal field states.

VIII. RESULTS: INCLUDING NONLOCAL INTERACTIONS

This section discusses our results for the Fermi surface average of the full quasiparticle scattering amplitude $\Gamma_{\rm QP}(\mathbf{k},\mathbf{k}')$ as given in Eq. (66). The functions $I_{ss\Gamma\Gamma'}(\mathbf{q})$, $I_{s\lambda\Gamma\Gamma'}(\mathbf{q})$, and $I_{\lambda\lambda\Gamma\Gamma'}(\mathbf{q})$ [see Eqs. (56)–(58)], contain the physics of the screened (by density fluctuations of the coupled conduction $4f$ electrons) slave bosons. The momentum dependence represents the contribution of nonlocal quasiparticles interactions in real space.

From Eqs. (66) and (65), we see that we must evaluate the self-energy functions for all unique combinations of $\mathbf{k}\pm\mathbf{k}'$. This we do separately from the actual averaging process. We store the required values for $I_{ss\Gamma\Gamma'}(\mathbf{q})$, $I_{s\lambda\Gamma\Gamma'}(\mathbf{q})$, and $I_{\lambda\lambda\Gamma\Gamma'}(\mathbf{q})$ in a look-up table. We saw in Sec. V that, due to the complicated effective matrix elements in cubic symmetry [see Eq. (60)], these functions are slowly converging numerical integrals, which prompted us to try the following line of attack. We have averaged the scattering amplitude [Eq. (66)] over the Fermi surface with a fixed *averaging* mesh. We vary, however, the mesh for calculating the bosonic Green function, as characterized by the parameter $n_{\rm mesh}$, and study the *average* interactions as a function of $n_{\rm mesh}$. With this procedure, it became clear that $n_{\rm mesh}\approx 50$ is a practical limit of the mesh size. Creating the look-up table for the bosonic self-energies would require well over a week of run time on a DEC5100 for anything bigger. Thus, it is important to ask if we can make any conclusions about possible pairing instabilities for $n_{\rm mesh}\leq 50$.

The values of Γ_η/T_{07} for $\eta=A_{1g}$ and $\eta=T_{2g}$ are plotted as a function of $n_{\rm mesh}$ in Fig. 7 for parameter set (a) and in Fig. 9 for parameter set (b). Also on the plots, the local values for the average are marked by horizontal lines for each representation (except A_{1g}). The results show the following.

(i) In the A_{1g} channel, the interactions are clearly repulsive. The nonlocal interactions, however, are attractive, since the average *local* repulsion is of the size $\Gamma_{{\rm local},A1g}/T_{07}$=3.54, and the inclusion of the momentum-dependent bosonic self-energy gives $\Gamma_{A1g}/T_{07}\approx 1.2$. Thus the nonlocal contribution has reduced the local repulsion by about a factor of 2, but is not sufficiently strong to yield a pairing instability.

(ii) In the T_{2g} channel, but for a glitch at $n_{\rm mesh}$=23, the interactions are repulsive for parameter set (a), with $\Gamma_{T2g}/T_{07}\approx$0.20. For parameter set (b) (Fig. 9), however, it is less clear if the average interaction is attractive or repulsive. Taking the results for both parameter sets together, we believe there is *no* pairing instability of T_{2g} symmetry.

The values of Γ_η/T_{07} for $\eta=E_g$ and $\eta=T_{1g}$ are plotted in Fig. 8 for parameter set (a) and in Fig. 10 for parameter set (b).

(i) The results for T_{1g} show attractive interactions, with an average value $\Gamma_{T1g}/T_{07}=-0.212\pm0.025$ for parameter set (a), and $=-0.226\pm0.049$ for parameter set (b).

(ii) The interactions in the E_g channel are less well behaved, but are attractive for $25\leq n_{\rm mesh}\leq 47$ [for parameter set (a)]. These numbers point to a possible superconducting instability of E_g symmetry, but the results have not converged enough for us to be sure. As a rough guide, using the numbers for $25\leq n_{\rm mesh}\leq 47$ would give $\langle\Gamma\rangle_{Eg}/T_{07}\approx$-0.163±0.054. The values for pa-

rameter set (b), however, have a surprisingly large fluctuation at n_{mesh}=31, which makes it very difficult to make any conclusion for $n_{\text{mesh}} \leq 35$. It is clear that the E_g states are the most sensitive to the fluctuations due to the anisotropic matrix elements in the bosonic self-energies, which includes the strongly peaking quasiparticle normalization function. From these results, we see that the T_{1g} pairing state is the most likely candidate for a pairing instability in cubic symmetry.

IX. DISCUSSION

As we have said, $n_{\text{mesh}} \approx 50$ is a practical limit on the size of the bosonic self-energy mesh that we could run on a local workstation. The appearance of fluctuations in the averaged scattering amplitude (Figs. 7–10), which limit our conclusions about possible pairing instabilities in cubic symmetry, is not shocking. After all, we know that there are fluctuations in the bosonic self-energies for $n_{\text{mesh}} \approx 80$. (See Fig. 5.) As we discussed, such variations are due to the anisotropic matrix elements in the principal value integrals over the Brillouin zone. If the matrix elements are sharply peaked in some region of the Brillouin zone, then it is easy to see how fluctuations can occur. If the mesh is constructed so that the matrix elements are evaluated very near a peak, then only a small shift in the mesh is required before the matrix elements will be evaluated at a point far down on the sides of the peak. Thus a small change in mesh size could result in a large change in the evaluated matrix elements.

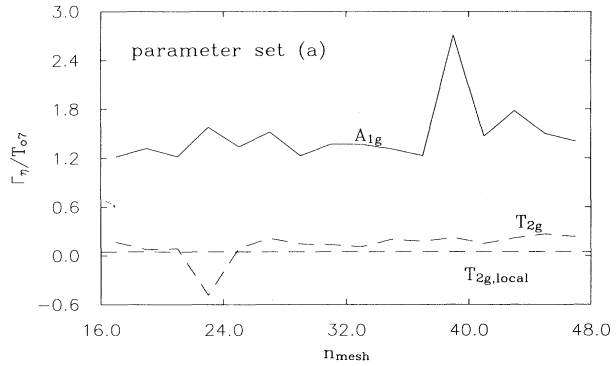

FIG. 7. Fermi surface averages in the A_{1g} and T_{2g} pairing channels of the scattering amplitude Γ_η/T_{07} as a function of the boson mesh parameter n_{mesh}. $8n_{\text{mesh}}^3$ equals the number of tetrahedra used in the Brillouin zone integrals for the bosonic Green functions. These data are for mean field parameter set (a). (See Table III.) (i) The horizontal line marked by $T_{2g,\text{local}}$ denotes the size of the local ("hard-core") contribution to the average in the T_{2g} channel. The corresponding local contribution for the A_{1g} channel is 3.54 and would be just above the top of the graph. We see that the nonlocal contribution in the T_{2g} channel is of the same size as the local contribution. Even with the fluctuation at n_{mesh}=23, it seems unlikely there is a pairing instability of T_{2g} symmetry. (ii) In the A_{1g} channel, even with the large fluctuation for n_{mesh}=39, there is clearly no pairing instability.

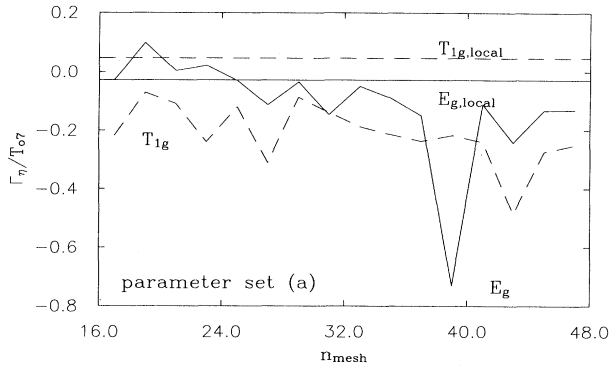

FIG. 8. Fermi surface averages in the E_{1g} and T_{1g} pairing channels of the scattering amplitude Γ_η/T_{07} as a function of the boson mesh parameter n_{mesh}. These data are for mean-field parameter set (a). The solid (dashed) horizontal line denotes the local contribution to the average in the E_g (T_{1g}) channel. (i) Although not yet converged, the averages in the T_{1g} channel point to the possibility of a pairing instability. Averaging the values of Γ_{T1g}/T_{07} for all the values of n_{mesh} used here yields $\frac{\Gamma_{T1g}}{T_{07}} = -0.212 \pm 0.025$. (ii) In the E_g channel, there is a large fluctuation at n_{mesh}=39. Therefore, we are hesitant to say that this is evidence of a superconducting instability. However, it is clear that the average interactions in this channel are attractive for a relatively wide range of mesh sizes: $25 \leq n_{\text{mesh}} \leq 47$.

A similar problem can arise in finite size lattice problems, where large variations in results can persist up to very large system sizes.[50] The solution for that particular problem is an average over boundary conditions. Our problem, unfortunately, has no such cure, and we must live with reasonable conclusions from the data we are

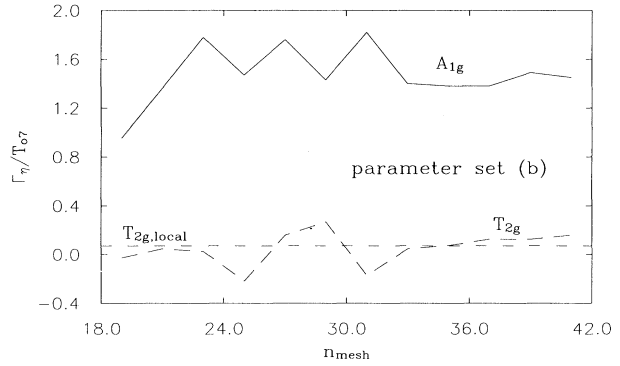

FIG. 9. Fermi surface averages in the A_{1g} and T_{2g} pairing channels of the scattering amplitude Γ_η/T_{07} as a function of the boson mesh parameter n_{mesh}. ($8n_{\text{mesh}}^3$ equals the number of tetrahedra used in the Brillouin zone integrals for the Bosonic Green functions.) These data are for mean-field parameter set (b). (i) In the T_{2g} channel, the horizontal, dashed line denotes the local contribution to the average. The fluctuations in the full average are at least a factor of 2 larger than the local part and are also varying about zero. Thus it is not possible to say, from the present data, if there is a T_{2g} instability or not. Using the results from parameter set (a), however, it still seems unlikely that there is an instability in this channel. (ii) In the A_{1g} channel, it is easy to see that there average interactions are repulsive and strong. There is no instability in this channel.

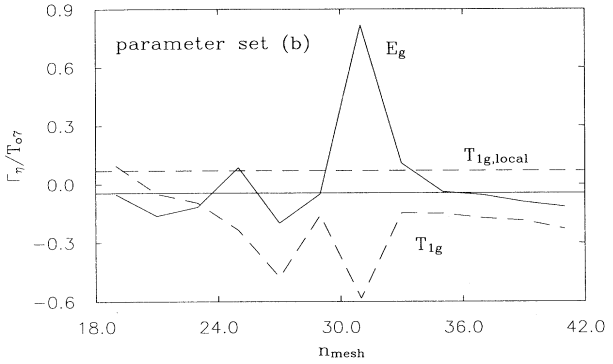

FIG. 10. Fermi surface averages in the E_{1g} and T_{1g} pairing channels of the scattering amplitude Γ_η/T_{07} as a function of the boson mesh parameter n_{mesh}. These data are for mean-field parameter set (b). (i) In the E_g channel, the horizontal line denotes the contribution to the average in the local limit. For the full average, up to n_{mesh}=31, the average value is fluctuating evenly about the local value. The surprisingly large fluctuation at n_{mesh}=31, however, makes it impossible to tell if there is an instability in this channel. (ii) In the T_{1g} channel, the full average, although fluctuating, remains negative for $21 \leq n_{\text{mesh}} \leq 41$. Averaging these values gives a result of $\frac{\Gamma_{T1g}}{T_{07}} = -0.226 \pm 0.049$.

able to gather.

To reiterate, we have been able to draw the following conclusions:

(i) States in the lowest quasiparticle band are strongly peaked at the Fermi surface hot spots, where hybridization between conduction and Γ_7 states vanishes.

(ii) The static susceptibility is dominated by the Pauli contribution from the Γ_7 states and yields a Wilson ratio of 2.38.

(iii) The best candidate for a pairing instability is in a state of T_{1g} $[xy(x^2+y^2)]$ symmetry, with $\Gamma_{T1g}/T_{07} = -0.212 \pm 0.025$.

(iv) The E_g channel $(x^2-y^2,\ 3z^2-r^2)$ also shows weak signs of an instability, with $\Gamma_{Eg}/T_{07} = -0.163 \pm 0.054$.

(v) Quasiparticle interactions are strong and repulsive in the A_{1g} ("s wave") pairing channel.

(vi) A pairing instability of T_{2g} $(xy,\ xz,\ yz)$ symmetry also appears highly unlikely.

(vii) Only pairing states of E_g symmetry are strongly affected by the presence of the six hot spots on the Fermi surface.

(viii) Including the dynamics of the bosons at order $1/N$, or performing a $1/N^2$ (static or dynamic) calculation is not presently possible due to the numerical complexities discussed above.

Using the classic weak-coupling equation for the superconducting transition temperature within a given representation η, we find (in the T_{1g} channel)

$$T_c(\eta = T_{1g}) = 1.13 T_{07} e^{T_{07}/\Gamma_{T1g}} \approx 0.09 \text{ K}, \qquad (71)$$

which is smaller than the measured T_c of $CeCu_2Si_2$. We did not expect, however, such a weak-coupling calculation to give a quantitatively accurate value for T_c, which leads us to say a few words about strong- versus weak-coupling results.

In the case of heavy fermions, the effective Fermi temperature is of the order of the Kondo temperature which is also the energy scale of importance for the superconducting glue. Thus, a strong-coupling calculation, including the energy dependence of the scattering amplitude, should be performed. Given the complexity of the static problem, however, including the dynamics of the slave bosons in the presence of crystal fields is not feasible. This does not necessarily imply that the pairing instabilities found in the static problem have no meaning. We shall discuss, generally, why this is so.

It is conventional wisdom,[51] that near the Fermi surface the quasiparticle self-energy for heavy fermions is strongly frequency dependent but only weakly dependent on the magnitude of the momentum, $|\mathbf{k}|$. This can be understood intuitively as follows. The characteristic energy scale for the quasiparticles is the Kondo temperature, T_{07}, which is about 10 K. The degeneracy temperature for a typical metal is $T_F \approx 10\,000$ K. The characteristic momentum, however, is set by the Fermi wave vector k_F, which for $CeCu_2Si_2$ is the size of the Fermi wave vector of a typical metal. Thus, broadly speaking, we expect the quasiparticle self-energy Σ to behave (near the Fermi surface) as

$$\frac{\partial \Sigma}{\partial \omega} \approx \mathcal{O}\left(\frac{\Sigma}{T_{07}}\right),$$

$$\frac{\partial \Sigma}{\partial \xi_{\mathbf{k}}} \approx \mathcal{O}\left(\frac{\Sigma}{D}\right),$$

where D is the bandwidth of the conduction band. Then, since

$$\frac{\partial \Sigma}{\partial \omega} \gg \frac{\partial \Sigma}{\partial \xi_{\mathbf{k}}},$$

it seems reasonable to ignore the momentum dependence of the self-energy. This intuitive result was reinforced by Millis and Lee,[11] who found [in the SU(N) model] that the momentum dependence of the imaginary part of the conduction electron self-energy (at order $1/N$) is very weak (going as $1/N^2$), while the frequency dependence goes as the inverse of the Kondo scale.

One may ask if the above inequality is valid near the hot spots, since we have seen a rapid variation of the quasiparticle normalization as a function of momentum in those regions. As mentioned before, the T_{1g} and T_{2g} pairing states are oblivious to what happens at the hot spots. Thus, even if $\partial\Sigma/\partial\omega \approx \partial\Sigma/\partial k$, this will have no affect on our conclusions about possible pairing instabilities in these channels. Results for local and nonlocal interactions in the vicinity of these areas imply that only the E_g pairing states might be affected. Thus, the only weakness in the argument of the preceding paragraph might be for the E_g states in the vicinity of the hot spots. But the slow convergence of the average quasiparticle interactions Γ_{Eg} has already prevented us from making a definitive statement about an E_g pairing instability. Thus, at the

present level of calculation, we believe this concern is secondary.

If one accepts the dominance of the frequency dependence in the quasiparticle self-energy, then it seems reasonable to assume that including such dependence in a strong coupling calculation (in the manner of McMillan[52]) would serve only to reduce the transition temperature T_c. We do not believe that the *sign* of the average scattering amplitude Γ_η would be affected by such frequency dependence. Thus, our conclusions about which pairing channels η show that a superconducting instability should not be changed as the result of a strong-coupling calculation.

Please note that we are *not* saying that the reduction of the transition temperature due to the frequency dependence of the residual quasiparticle interactions would be identical in structure to the case of electron-phonon coupling.[52] We can only say now that we expect T_c to be reduced; we cannot give an estimate of how large the reduction would be.

The superconducting instabilities themselves appear to be based heavily on the underlying symmetry of the problem. The fact that our estimated (weak-coupling) transition temperature for the T_{1g} pairing instability differs from the measured value for $CeCu_2Si_2$, is not a surprise. The major purpose of this calculation has not been to give a precise numerical recipe for calculating the T_c of heavy fermion systems. We wished to study the importance of local, or "multiplet," physics upon quasiparticle interactions. Thus the weak-coupling calculation should be a reasonable starting point.

We close with a few general words on the importance of the excited crystal field levels on quasiparticle interactions. The following statements should be applicable to crystal-field-split heavy fermion compounds, not just $CeCu_2Si_2$. We require only that the system can be modelled by an infinite-U periodic Anderson model. There are three broad characteristics that determine the nature of the interactions and the importance of the excited crystal field multiplets to those interactions: (1) the ratio of the ground multiplet Kondo temperature to the crystal field splitting ($T_{0\Gamma}/\Delta_{\rm CEF}$), (2) the point symmetry at the rare-earth or actinide sites, (3) and the degeneracy of the low-lying multiplet as compared to the degeneracy of the conduction bands.

The first characteristic is probably the most important of the three. As discussed in Ref. 22, the contribution to the *local* quasiparticle interactions due to the excited crystal field levels is reduced in strength by the factor $(T_{0\Gamma}/\Delta_{\rm CEF})^n$ (n=1 or 2) when compared to the interaction strength when only the ground multiplet is included. Experience with calculations pertaining to $CeCu_2Si_2$, for which $T_{0\Gamma}/\Delta_{\rm CEF}\approx 0.03$, leads us to believe that values of this ratio more than an order of magnitude smaller than the estimate for $CeCu_2Si_2$ result in a negligible contribution to the *local* interactions from the excited multiplets. Furthermore, this ratio determines the angular width in momentum space of the hot spot peaks. (See Fig. 2.) Thus as $T_{0\Gamma}/\Delta_{\rm CEF}$ becomes smaller, the peaks narrow and the effects on quasiparticle interactions should decrease.

The second characteristic determines where in the Brillouin zone the hot spots will occur and which representations of the point group will be most sensitive to the details of the spots. Since these spots correspond to $\mathbf{k}$ values at which the ground (excited) multiplet cannot hybridize, in these regions the hybridization of the excited (ground) multiplet with the conduction states gives rise to the quasiparticle interactions.

The third characteristic is part of a simplified "rule of thumb" that we found to be helpful in understanding our results for $CeCu_2Si_2$. When the ground multiplet has a degeneracy equal to that of the conduction states, in a very rough sense the problem has reduced to a SU(N) model (with N=2 for $CeCu_2Si_2$). Then one might guess that the results of Lavagna, Millis, and Lee[15] would be reasonable, in which the only local interactions are repulsive and s wave in character. The extent to which such a SU(N)-like result is modified by the presence of the excited multiplet depends mostly on the size of the ratio $T_{0\Gamma}/\Delta_{\rm CEF}$. If, however, the ground multiplet has a degeneracy greater than that of the conduction states, then a subset of the multiplet states cannot hybridize, and the situation is analogous to the jellium model of Zhang and Lee.[17] In this case, we would expect local interactions to be repulsive in angular momentum channels higher than just s wave, thereby reducing the overall chances of any pairing instability.

ACKNOWLEDGMENTS

The author wishes to thank D. L. Cox for invaluable guidance and support over the duration of this project. The author also wishes to thank the following people for meaningful discussions: J. W. Wilkins, C. Pennington, M. Alouani, and M. Steiner. This work was supported by a grant from the U.S. Department of Energy, Office of Basic Energy Sciences, Division of Materials Research.

* Present address: Department of Physics, Monmouth College, Monmouth, Illinois 61462.

[1] F. Steglich, J. Aarts, C. D. Bredl, W. Lieke, D. Meschede, W. Franz, and H. Schäfer, Phys. Rev. Lett. **43**, 1892 (1979).
[2] N. Grewe and F. Steglich, in *Handbook on the Physics and Chemistry of Rare-Earths*, edited by K. A. Gschneider, Jr. and L. Eyring (North-Holland, Amsterdam, 1990), Vol. 14.
[3] G. R. Stewart, Rev. Mod. Phys. **56**, 755 (1984).
[4] P. A. Lee, T. M. Rice, J. W. Serene, and J. W. Wilkins, Comments on Condens. Matter. Phys. **12**, 99 (1986).
[5] B. Welslau and N. Grewe, Ann. Phys. (Leipzig) **1**, 214 (1992).

[6] P. Fulde, J. Keller, and G. Zwicknagl, Solid State Phys. **41**, 1 (1988).
[7] D. Rainer, Phys. Scr. T **23**, 106 (1988).
[8] S. E. Barnes, J. Phys. F **6**, 1375 (1976).
[9] N. Read and D. M. Newns, J. Phys. C **16**, L1055 (1983).
[10] P. Coleman, Phys. Rev. B **29**, 3035 (1984).
[11] A. J. Millis and P. A. Lee, Phys. Rev. B **35**, 3394 (1986).
[12] A. Auerbach and K. Levin, Phys. Rev. Lett. **57**, 877 (1986).
[13] Z. Tešanović and O. T. Valls, Phys. Rev. B **34**, 1918 (1986).
[14] P. Coleman, Phys. Rev. B **35**, 5072 (1987).
[15] M. Lavagna, A. J. Millis, and P. A. Lee, Phys. Rev. Lett. **58**, 266 (1987).
[16] A. Houghton, N. Read, and H. Won, Phys. Rev. B **35**, 5123 (1987).
[17] F. C. Zhang and T. K. Lee, Phys. Rev. B **35**, 3651 (1987).
[18] B. Coqblin and J. R. Schrieffer, Phys. Rev. **185**, 847 (1969).
[19] Z. Zou and P. W. Anderson, Phys. Rev. Lett. **57**, 2073 (1986).
[20] P. Schlottmann, Phys. Rep. **181**, 1 (1989).
[21] J. W. Rasul and A. C. Hewson, J. Phys. C **17**, 3337 (1984).
[22] B. R. Trees and D. L. Cox, Phys. Rev. B **49**, 16066 (1994).
[23] N. Read and D. M. Newns, J. Phys. C **16**, 3273 (1983).
[24] C. D. Bredl, W. Lieke, R. Schefzyk, M. Lang, U. Rauchschwalbe, F. Steglich, S. Riegel, R. Felten, G. Weber, J. Klaasse, J. Aarts, and F. R. de Boer, J. Magn. Magn. Matter **47&48**, 30 (1985).
[25] F. Steglich, U. Rauchschwalbe, U. Gottwich, H. M. Mayer, G. Sparn, N. Grewe, U. Poppe, and J. J. M. Franse, J. Appl. Phys. **57**, 3054 (1985).
[26] U. Rauchschwalbe, Physica **147B**, 1 (1987).
[27] S. Horn, E. Holland-Moritz, M. Loewenhaupt, F. Steglich, H. Scheuer, A. Benoit, and J. Flouquet, Phys. Rev. B **23**, 3171 (1981).
[28] K. R. Lea, M. J. M. Leask, and W. P. Wolff, J. Phys. Chem. Solids **23**, 1381 (1962).
[29] J. S. Kang, J. W. Allen, O. Gunnarsson, N. E. Christensen, O. K. Andersen, Y. Lassailly, M. B. Maple, and M. S. Torikachvili, Phys. Rev. B **41**, 6610 (1990).
[30] R. D. Parks, M. L. den Boer, S. Raaen, J. L. Smith, and G. P. Williams, Phys. Rev. B **30**, 1580 (1984).
[31] D. L. Cox (unpublished).
[32] R. M. Martin, Phys. Rev. Lett. **48**, 362 (1982).
[33] See, e.g., P. Fulde, *Electronic Correlations in Molecules and Solids* (Springer-Verlag, Berlin, 1991), p. 44.
[34] D. L. Cox, Phys. Rev. Lett. **59**, 1240 (1987).
[35] B. Batlogg, J. P. Remeika, A. S. Cooper, and Z. Fisk, J. Appl. Phys. **55**, 2001 (1984).
[36] F. C. Zhang and T. K. Lee, Phys. Rev. Lett. **58**, 2728 (1987).
[37] G. Aeppli and C. M. Varma, Phys. Rev. Lett. **58**, 2729 (1987).
[38] O. Jepsen and O. K. Andersen, Solid State Commun. **9**, 1763 (1971).
[39] G. Lehmann, P. Rennert, M. Taut, and H. Wonn, Phys. Status Solidi **37**, K27 (1970).
[40] J. Rath and A. J. Freeman, Phys. Rev. B **11**, 2109 (1975).
[41] Per-Anker Lingård, Solid State Commun. **16**, 481 (1975).
[42] D. L. Cox, Ph.D. thesis, Cornell University, 1985.
[43] G. Gilat, J. Comput. Phys. **10**, 432 (1972).
[44] G. Gilat, in *Methods in Computational Physics*, edited by G. Gilat, B. J. Alder, S. Fernbach, and M. Rotenberg (Academic, New York, 1976), Vol. 15.
[45] Matthew Steiner (private communication).
[46] K. Asayama, Y. Kitaoka, and Y. Kohori, J. Magn. Magn. Mater. **76&77**, 449 (1988).
[47] K. Ueda and T. M. Rice, Phys. Rev. B **31**, 7114 (1985).
[48] S. L. Altmann and A. P. Cracknell, Rev. Mod. Phys. **37**, 19 (1965).
[49] B. R. Trees, Ph.D. thesis, The Ohio State University, 1993.
[50] K. -H. Luk and D. L. Cox, Phys. Rev B **41**, 4456 (1990).
[51] C. M. Varma, Phys. Rev. Lett. **55**, 2723 (1985).
[52] W. L. McMillan, Phys. Rev. **167**, 331 (1968).